UNIVERSIDADE FEDERAL DO RIO GRANDE DO SUL
ENGINEER SCHOOL
MATERIALS ENGINEERING

ENG 02298 – BACHELOR THESIS

ANALYSIS OF ORBITAL FLOOR BLOWOUT FRACTURES USING ANONYMIZED COMPUTED TOMOGRAPHY SCANS

Antoniella Ingrassia
00243766

Adviser: Professor Dr. Luís Alberto Loureiro dos Santos
Co-advisor: Dr. Cindy Elschner

Porto Alegre
October 2021.

ANTONIELLA INGRASSIA

ANALYSIS OF ORBITAL FLOOR BLOWOUT FRACTURES USING ANONYMIZED COMPUTED TOMOGRAPHY SCANS

End of course work presented to the Materials Engineering Graduate Course at Universidade Federal do Rio Grande do Sul, as partial requirement for obtaining the title of Materials Engineer.

Adviser: Prof. Dr. Luis Alberto Loureiro dos Santos
Co – adviser: Dr. Cindy Elschner

Porto Alegre
October 2021.

ACKNOWLEGMENT

First, I especially thank my parents Adriano Ingrassia and Simone Ingrassia. My father for teaching me what is right and wrong, for his guidance in all my most difficult choices and decisive moments, my mother for showing how to be a strong, confident, and determined woman. Without all their love, trust, emotional and financial support I would not have done and conquered everything I have achieved so far. They are the example of upright, dedicated, resilient and empathetic people that I will follow all my life. Everything I do is to make you proud and make your efforts worth, thank you so much.

I thank my family, my aunt Tatiana Detzel for being a little bit of everything for me during my whole life: my friend, my sister, my mother and even my personal adviser, my uncle Alexandre Ingrassia for his love and enthusiasm for my achievements, my grandparents specially Maria de Lourdes, a big love of my life, the one who always had love, wisdom words and also lunches ready for me during my rush days of classes, with a call of distance. My cousin Giovanna Ingrassia with all her motivation for being independence and teach me that family always comes first no matter what.

I would like to thank my supervisor and co-adviser, Dr. Cindy Elschner for choosing and trusting me on this subject in such a difficult moment for the world. I also want to thank her for inspiring me to continue in the research field which is something I was already passionate about. I also thank for the incredible welcome and hospitality provided by the Leibniz-Institute für Polymerforschung, where I did this work, they made me feel at home.

I thank my adviser Prof. Dr. Luís Alberto Loureiro dos Santos for the excellent teaching on biomaterials in my undergraduate classes, for the opportunity to have worked in this area and learned so much and for his guidance on the present work.

I also want to thank Dr. Fernanda Vecchietti with whom I had the pleasure of working before coming to the Institute in the same field of biomaterials and made me learn a lot. Without her I would never have got this incredible opportunity to work and study in this renowned Institute.

I thank the opportunity to have study in one of the best universities of Brazil, federal, especially in the current reality of our country, where many don't have this privilege. When I think of the person I was when it all started and look at the person I am today, I know that the University as well as everything that was provided to me because of it has made me a better person, more critical, more analytical, and much more aware of my duties and responsibilities as an individual and as a citizen.

I thank my graduation colleagues, especially Carolina Delwing, Kimberllyn Pereira, João Pedro Weiss and Diogo Carvalho, for their friendship and partnership during the long semesters with endless exams – the professors, and laboratories inside de University where I worked during the graduation time – Advanced Biomaterials and Ceramics Laboratory and Physical Metallurgy Laboratory -, I learned so much with all of you. My eternal gratitude for all the teachings and knowledge exchanged.

I am grateful for all my friends and for the people that I found in my path and were so helpful and kind to me in a lot of ways. Dr. Tales de Vargas Lisbôa, Luciana Lamb, Atmika Bhardwaj, João Vitor Dias Honorato de Oliveira and Guilherme Auwarter, they were my second family when I was away from Brazil and helped me through all my challenges, including this work.

And finally, I think my friends Betina Bramraiter Borile, Lucke Severino Teixeira and Isabella Casco for their help in times of need, kindness, and trust before and during this journey, throughout high school, university, and I hope in all the other steps that will come.

ABSTRACT

The orbits are bony structures of the skull that house the globe, extraocular muscles, nerves, blood vessels, lacrimal apparatus, and adipose tissue. Each orbit protects the globe, while the supportive tissues allow the globe to move in three dimensions (horizontal, vertical, and torsional). The orbital floor comprises the maxillary, palatine, and zygomatic bones, and the walls of the orbit function as a physical barrier from blunt trauma to the eye, an anchor for muscles and ligaments to attach, and additionally serve as a window for neurovasculature to travel through. Because of its position and its thin bony walls, it is susceptible to fractures, and in a lot of cases surgery is required as part of the treatment to repair the resulting defect with an implant. In this context, the present work had the purpose to analyze medical computed tomography (CT) and cone beam computed tomography (CBCT) – also called digital volume tomography (DVT) - imaging data from anonymized patients with orbital floor defects for the measurement of the length, the depth, the total area, and the defect area of them using the software called VG STUDIOMAX (Volume Graphics GmbH, Heildelberg, Germany) designed for industrial CT examinations. The analysis of medical imaging data is equally possible, but new for the case of orbital floor defects. The method was successfully done, and some of the results obtained on this work are similar to the values obtained on the literature. The main values obtained for length measurements of total orbital floor were 28,18 ± 2,93 mm and 27,93 ± 2,70 mm for left and right side respectively (p = 0,83). The main values obtained for depth measurements of total orbital floor were 29,80 ± 2,80 mm and 29,40 ± 3,03 mm for left and right side respectively (p = 0,74). The main values obtained for length and depth of orbital floor defects were 13,61 ± 4,98 and 17,38 ± 5,82 respectively (p = 0,14). By conventional criteria, these differences are considered to be not statistically significant showing reproducible results, however, no studies were found to compare it with. The main values obtained for total surface area were 632,89 ± 147,44 mm² and 641,76 ± 150,09 mm² for left and right side respectively (p = 0,88) and the main value obtained for defect surface area 403,28,32 ± 132,15 mm², being similar to other studies. The mean value for defect and total area ratio obtained on this work, 65,00 ± 15,00, a little higher than the ones calculated on the other studies found in literature.

Keywords: orbital floor, orbital floor fractures, measurement, analysis, CT scans.

RESUMO

As órbitas são estruturas ósseas do crânio que abrigam o globo terrestre, músculos extraoculares, nervos, vasos sanguíneos, aparelho lacrimal e tecido adiposo. Cada órbita protege o globo ocular, enquanto os tecidos de suporte permitem que o globo se mova em três dimensões (horizontal, vertical e de torção). O piso (ou assoalho) orbital compreende os ossos maxilares, palatinos e zigomáticos, e as paredes da órbita funcionam como uma barreira física contra traumas no olho, uma âncora para os músculos e ligamentos se fixarem, e adicionalmente servem como uma janela para a neurovasculatura viajar através. Devido a sua posição e suas finas paredes ósseas, é suscetível a fraturas e, em muitos casos, é necessária cirurgia como parte do tratamento para reparar o defeito resultante com um implante. Neste contexto, o presente trabalho teve a finalidade de analisar imagens de tomografia computadorizada médica (TC) e de tomografia computadorizada de feixe cônico (TCFC) - também chamada tomografia digital de volume (TDV) – de pacientes anônimos com defeitos no piso orbital para a medição do comprimento, da profundidade, da área total e da área defeituosa dos mesmos, utilizando o software chamado VG STUDIOMAX (Volume Graphics GmbH, Heildelberg, Alemanha) projetado para exames de TC industriais. A análise de dados de imagens médicas é igualmente possível, mas nova para o caso de defeitos orbitais do piso. O método foi realizado com sucesso e alguns dos resultados obtidos neste trabalho são semelhantes aos valores obtidos na literatura. Os valores médios obtidos para as medidas de comprimento do piso orbital total foram 28,18 ± 2,93 mm e 27,93 ± 2,70 mm para os lados esquerdo e direito respectivamente (p = 0,83). Para as medidas de profundidade do piso orbital total obteve-se 29,80 ± 2,80 mm e 29,40 ± 3,03 mm para os lados esquerdo e direito respectivamente (p = 0,74). Para as medidas de comprimento e profundidade dos defeitos do piso orbital obteve-se 13,61 ± 4,98 e 17,38 ± 5,82 respectivamente (p = 0,14). Por critérios convencionais, estas diferenças são consideradas como não estatisticamente significativas mostrando resultados reprodutíveis, entretanto, não foram encontrados estudos para compará-los. Os valores obtidos para a área de superfície total foram 632,89 ± 147,44 mm^2 e 641,76 ± 150,09 mm^2 para os lados esquerdo e direito respectivamente (p = 0,88) e o valor obtido para a área de superfície do defeito foi 403,28 ± 132,15 mm^2, sendo similares

a outros estudos. O valor médio para a razão entre o defeito e a área total obtido neste trabalho foi de 65,00 ± 15,00, um pouco maior do que os valores calculados em outros estudos encontrados na literatura.
Palavras-chave: piso orbital, fraturas do piso orbital, medições, análises, imagens de TC.

LIST OF FIGURES

LIST OF TABLES

LIST OF ACRONYMS AND ABBREVIATIONS

CT	Computed tomography
CBCT	Cone beam computed tomography
DICOM	Digital imaging and communications in medicine
DVT	Digital volume tomography
ISO	International Organization for Standardization
HA	Hydroxyapatite
HT	Hydraulic theory
OBF	Orbital floor fracture
OFD	Orbital floor defects
OFS	Orbital floor surface
PE	Polyethylene
PLA	Poly (lactic acid)
PLLA	Poly-L-lactide
PSI	Patient specific implant
PSL	Posterior shelf length
PGA	Poly (glycolic acid)
ROI's	Regions of Interest
SD	Standard deviation
VG	Volume Graphics
2D	Bidimensional
3D	Tridimensional

GLOSSARY

Assessment	The evaluation or estimation of the nature, quality, or ability of someone or something
Enophthalmos	Infra-position of the globe
Diplopia	Double vision of the eye
Hypoglobus	The loss of anterior support to the globe that can result in vertical displacement of the globe
Coronal view	Same as a frontal view of an object
Sagittal view	Same as a lateral view of an object
Transversal view	Top-under view of and object
Orbital rim	The anterior edge of the bony orbit, or eye socket, formed by the maxilla and zygomatic bone inferiorly and the frontal bone superiorly
Orbital apex	The posterior confluence of the orbit at the craniofacial junction, where nerves and vessels are transmitted from the intracranial compartment into the orbit via several bony apertures, the point where the extraocular muscles derive their origins

LIST OF CONTENTS

1 INTRODUCTION

The orbits are bony structures of the skull that house the globe, extraocular muscles, nerves, blood vessels, lacrimal apparatus, and adipose tissue. Each orbit protects the globe, while the supportive tissues allow the globe to move in three dimensions (horizontal, vertical, and torsional). The orbital floor comprises the maxillary, palatine, and zygomatic bones, and the walls of the orbit function as a physical barrier from blunt trauma to the eye, an anchor for muscles and ligaments to attach, and additionally serve as a window for neurovasculature to travel through. Because of its position and its thin bony walls, it is susceptible to fractures.

The management of patients with orbital processes can be challenging due to the wide variety of diseases that can develop as an intrinsic problem, as direct extension from cranial, bony, sinonasal, and cutaneous origins, as well as from distant sources (e.g., hematogenous spread of infection or metastatic disease from lung, prostate, or breast) (KHAN et al, 2006).

The most commonly midfacial fractures are in the orbital floor, alone or with other facial skeletal damage. In this context, most of the times it is necessary to do treatments to fix the fractures, and big part of them involving surgical procedures and the use of implants. Within the years, studies have been made to improve the results and probable permanent damages of it, but it remains very complex to achieve that due to the complexity of the problem. It takes multidisciplinary knowledge such as medical – including maxillofacial, otolaryngological and ophthalmic fields – and an engineering part – consisted of the study of the better material and its properties for the implant when its needed, along with a specific size shaped for each patient.

The present work was developed as part of an ongoing project at the Leibniz-Institute für Polymerforschung Dresden e.V. within the Bioengineering group that studies embroidery processing of ultra-thin titanium wires for the development of patient-specific, shapeable orbital floor implants. The goal here was to analyze medical computed tomography (CT) and cone beam computed tomography (CBCT) imaging data of anonymized patients with orbital floor defects for the measurement of the length, the depth, the total area, and the defect area of them using the software called VG STUDIOMAX by Volume Graphics (Volume Graphics, Heidelberg, Germany), used for industrial applications. The analysis of medical imaging data is equally possible, but new for the case of orbital floor defects using this software. This was the first step for the further development of a more accurate size and shape orbital floor implants along with the best material option.

To be able to do the measurements properly, a literature review was done previously covering orbital floor fracture - etiology, treatment, and materials for implants -, orbital floor fractures measurements and study of the software VGSTUDIO MAX.

2 OBJECTIVES

General objective: analysis of orbital floor blowout fractures using anonymized computed tomography (CT) and cone beam computed tomography (CBCT) scans.

Specific objectives:

- Study of orbital floor fractures, including etiology, treatment, and materials for reconstruction;
- Study of methodologies for orbital floor measurements;
- Perform measurements on the orbital floor using the industrial-use software VGSTUDIO MAX, analyze the results statistically, and compare them with literature.

3 LITERATURE REVIEW

The orbit is a pear shape, with the optic nerve at the stem. The entrance to the globe anteriorly is approximately 35 mm high and 45 mm wide. The depth from orbital rim to the orbital apex measures 40 to 45 mm in adults. The maximum width is 1 cm behind the anterior orbital margin. Both race and gender can affect the measurements of the bony orbit. The orbital cavity contains the globe, nerves, vessels, lacrimal gland, extraocular muscles, tendons, and the trochlea as well as fat and other connective tissue and the following seven bones form the orbit: sphenoid, frontal zygomatic, ethmoid, lacrimal, maxilla and palatine (SHUNMWAY et al, 2021).

Figure 1: The bones of the orbit and associated extraocular muscles and nerves.

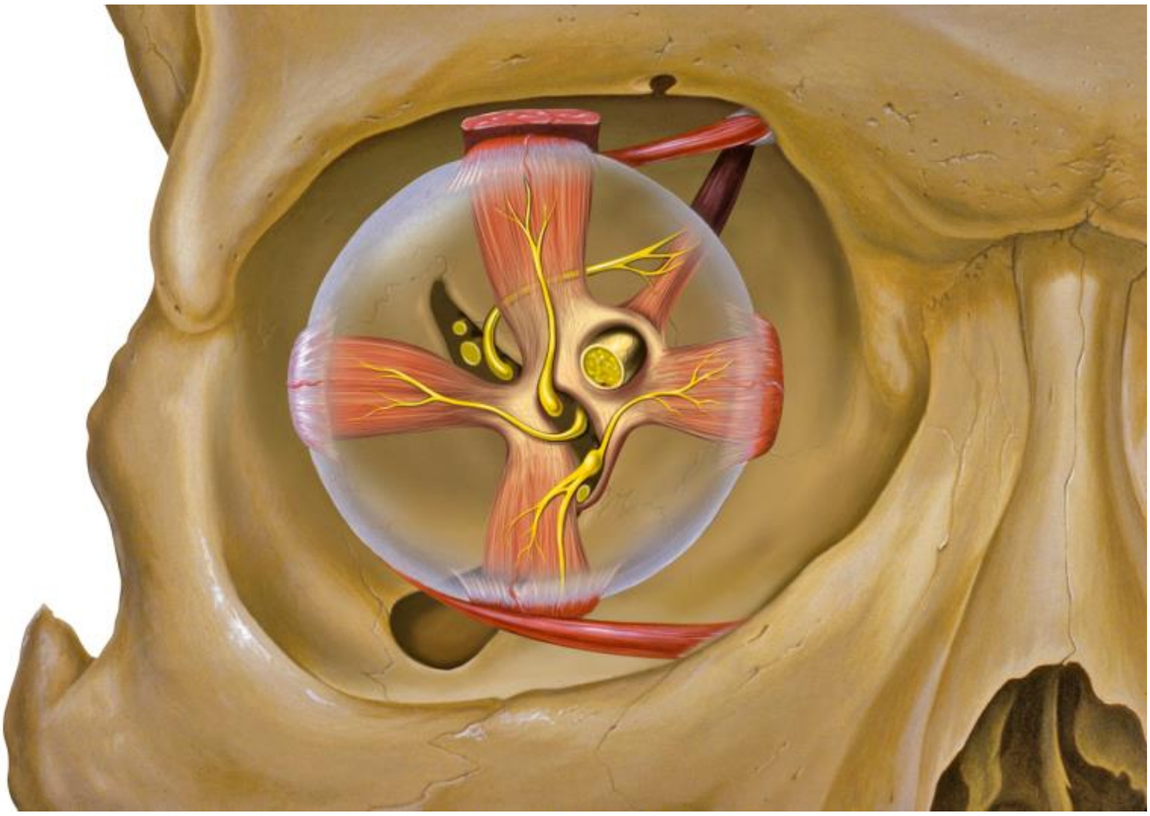

Source: SHUNMWAY et al, 2021.

Figure 2: Orbital bones.

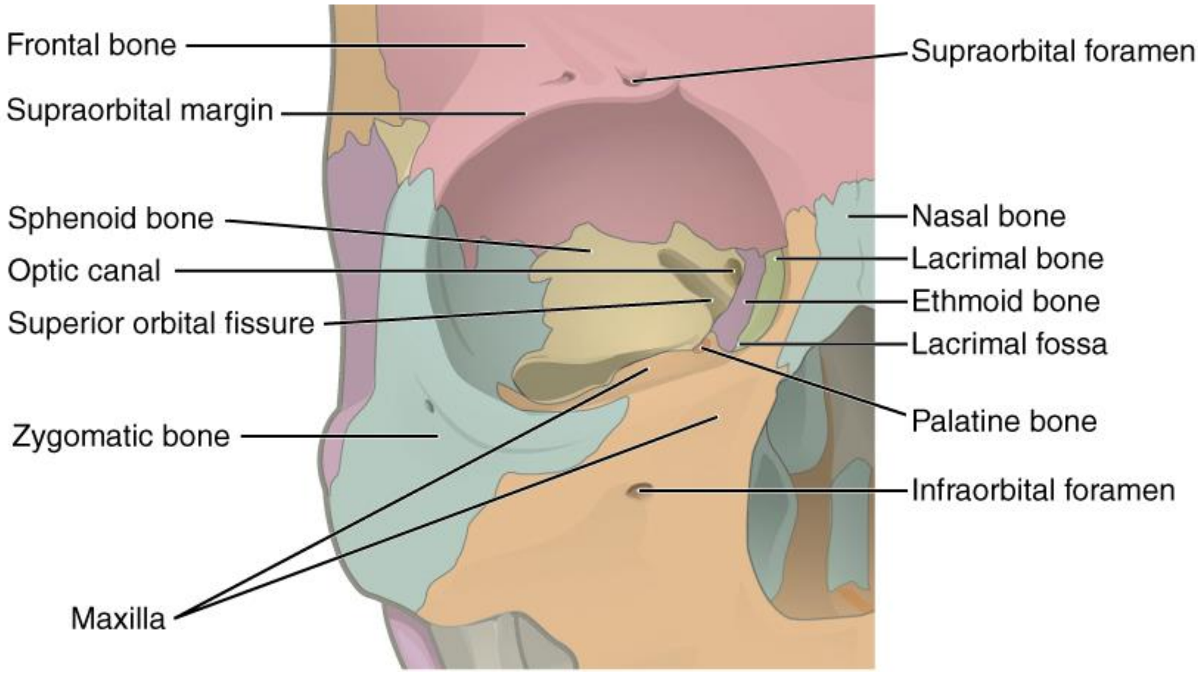

Source: Case courtesy of OpenStax College, Radiopaedia.org, rID: 42758.

3.1 ORBITAL FLOOR FRACTURES

The repair of cranial defects is necessary to provide neural protection and is aesthetically desirable. Tumors, trauma, disease, and congenital defects generate the need for bone reconstruction. The treatment of craniofacial defects is a challenge for the surgical team, and often involves multiple surgeries, some at high cost, but in some cases the results obtained are not satisfactory, and in this sense, there is a continuous concern in the improvement and development of new treatment methodologies. (BERTOL, 2008).

Orbital fractures usually occur due an external impact of low, medium, or high velocity trauma by an interpersonal violence, a vehicle or traffic accident. It often consists of the combination of buckling forces applied to the orbital rim and/or the retropulsion of orbital content. Consequently, this impact may result in comminution of the walls and dislocation of bone fragments into the adjacent sinuses. Although orbital floor fractures can occur in combination with other facial bony disruption, approximately half of all orbital fractures consist of isolated wall fractures, predominantly orbital floor, and medial wall fractures. The isolated orbital fractures commonly result from an impact injury to the ocular globe and upper eyelid (DUBOIS, 2016).

The review for etiology, treatment and materials for orbital floor reconstruction are presented below:

3.1.1 Etiology

According to literature studies, different biomechanical theories can explain the injury of orbital floor blowout fractures and they are not only of academic interest but also of clinical importance in terms of prevention and treatment. (RHEE et al, 2002).

The theories are explained below:

1) Hydraulic Theory (HT), which involves the direct transmission of pressure from the ocular globe and intra-orbital content to the peri-ocular structures, which eventually leads to blowing out of the orbital floor. In other words, increased orbital content pressure results in direct compression of the orbital floor and therefore causing a fracture of the thin bone. (RHEE et al, 2002).

   RHEE et al (2002), examined the pure hydraulic mechanism (absence of orbital rim or facial skeleton trauma) of injury using a 1-kg pendulum to strike fresh human cadaver heads at a range of drop heights and found that isolated orbital floor fractures were obtained at lower heights and at lower threshold for fracture than the medial wall.

2) Transmission Theory: assumes that the isolated orbital floor fracture is a result of the force acting on the orbital rim. The application of force to the orbital rim can cause compression and curvature of the orbital floor, and as a result, it fractures (JIANG, 2020).
3) Bone Conduction Theory (BCT), which involves indirect transmission of pressure from the orbital rim along the bone to the floor. It suggests that a force, not powerful enough to fracture the rim, will propagate along the bone to fracture the weaker orbital floor (BOYETTE et al, 2015).

Clinical symptoms are associated with orbital fractures, the most common like as follow, due a prolapse of the orbital content and displacement of the eye globe into the maxillary sinus cavity. It has been previously reported that enlargement and deformation of the orbit give rise to enophthalmos and therefore, disturbance of eye motility together with double images is likely to occur (JAQUIÉRY, 2007). Enophthalmos may not be apparent immediately after trauma due to edema and swelling but becomes apparent by 5–7 days after injury and should be evaluated then (HOYT AND TAYLOR, 2013).

Furthermore, there are three main types of orbital fracture, described below (BOYETTE et al, 2015; ROTH et al, 2010; BOYD, 2017):

1) Orbital rim fracture: it is a fracture of the bony, thick outer edges of the eye socket and so it requires a lot of force and usually presents with multiple other facial injuries and can also damage the optic nerve.
2) Direct orbital floor fracture: it is a rim fracture that has extended into the floor and occurs when a blow or a trauma to the orbital rim pushes the bones back and causes the floor eye socket to buckle and break being possible to affect muscles and nerves around the eye.
3) Indirect orbital floor fracture ("blowout fracture"): it is a crack in the inner wall or floor of the eye socket, and it is the most common orbital type of fracture. It occurs due to blunt force trauma by something that is bigger than the eye and can impinge on the eye muscles and surrounding anatomy, potentially interfering with the eye movement.

The symptoms are going to vary based on the type of fracture, but can include (BOYETTE et al, 2015; ROTH et al, 2010; VIOZZI, 2017; BOYD, 2017):

- A black eye;
- Swelling and discoloration around the eye;
- Redness and bleeding on the whites of the eyes and inner eyelid;
- Swelling or deformity of the forehead and/or cheek, with an obvious indent over the broken bone;
- Diplopia (double vision);
- Limited ability to look in certain directions;
- Numbness or change in sensation on the side of the injury (possibly related to nerve damage);
- An abnormally flat-looking cheek;
- Sinking or bulging of the eyeballs (the latter is known as exophthalmos);
- Severe pain in the cheek when opening the mouth.

3.1.2 Treatment

If indicated, the outer orbital frame is reconstructed by repositioning the bony fragments into their original position and fixating them with osteosynthesis materials. However, for the orbital walls, the goal of reconstruction is to lift the globe into its original position by placing an orbital implant to recontour the traumatized orbit and restore the traumatized anatomy as accurately as possible. True orbital reconstruction may be difficult due to the complex anatomy involved and the lack of an overview, which potentially leads to an unpredictable outcome. Furthermore, even if anatomical reconstruction is achieved, functional rehabilitation does not always occur as trauma to soft tissue contents may cause effects such as scarring, entrapment and fat atrophy (DUBOIS, 2016).

The timing of repair and modality of surgical intervention are critical issues that will strongly affect the results of orbital floor fracture treatment. Depending on each case, immediate surgical treatment is recommended, surgical repair within 2 weeks or medical therapy. For surgery cases, it is important that the patient knows all the possible risks and complications of an orbital reconstruction and not just the best restoration should be considered, but also cosmetic appearance and visual function. Partial or total loss of vision is the most dramatic complication that may occur and often directly related to the implant, such as extrusion, infection, or chronic inflammation, which can also require extra surgery to remove the foreign material. Also, a careful history and physical examination of the patient is vital for the diagnosis of orbital floor fractures and knowing the size/shape of the damage (BAINO, 2011).

The surgical approaches to the orbit are designed to enable the most direct access to the lesion/area of interest and depend on the location of the lesion within the orbit (KHAN et al, 2006).

3.1.3 Materials for orbital floor reconstruction

An ideal implant biomaterial should be (i) biocompatible, (ii) available in sufficient quantities, (iii) strong enough to support the orbital content and the related compressive forces, (iv) easy to shape to fit the orbital defect and regional anatomy, (v) easily fixable in situ, (vi) not prone to migration, (vii) osteoinductive and (viii) bioresorbable with minimal foreign body reaction (BAINO, 2011).

Nowadays a wide variety of types of biomaterials have been searched on literature for repairing of orbital floor. SAMMAN (2013) and BAINO (2011) did reviews for biomaterials for implants and repair of orbital floor defects such as biological, bioceramics, metals, polymers, and composites:

1) Biologicals: this are the ones derived from human or animal tissues that could be used as transplants or treated to obtain an implant. The usual types of biological materials are the ones listed next:
    a. Autografts: requires autologous patient tissue harvested from a donor site, shaped to match the defect dimensions. Most common used are autologous bone (consider the “golden standard”) and cartilage (ear and nasal septum).
    b. Allografts: transplant of hard/soft tissues from another living patient or from a cadaver.
    c. Xenografts: animal derived.
2) Bioceramics: Hydroxyapatite (HA) due to its chemical and crystallographic similarity to bone mineral is an excellent material for bone defect repair, including orbital floor defects. Custom-made HA implants can be fabricated by computer-aided design using data obtained through CT, which provides high anatomical accuracy.

    Another bioceramics used is bioactive glass that has a unique property of bonding to bone and stimulating new bone growth. Bioactive silica glass is bacteriostatic and more rigid than other materials and has potential as an orbital implant, but it is difficult to customize (KIM et al, 2016).
3) Metals: Titanium is highly biocompatible and due to its phyco-mechanical properties, is an ideal candidate for the reconstruction of bone defects requiring substitutes with high rigidity and strength and it’s also suitable for large orbital fractures. A lot of studies reported that it has no or minimal post-operative infections in patients. Another type of metal possible is cobalt chrome alloys due to its high resistance to corrosion but it is not much used for orbital floor repair.
4) Polymers: Many different polymers can be used such as silicone, polyethylene (PE), polytetrafluorethylene, nylon, hydrogels, poly (lactic acid) (PLA) / poly (glycolic acid) (PGA).

Poly-L-lactide (PLLA) and polyglycolic acid (PGA) are absorbable implants with sufficient biomechanical resistance for orbital wall reconstruction. Both are malleable and impermanent and in time are replaced by bone. The drawbacks of PLLA and PGA implants are radiolucency, the possibility of inflammation with degradation, limited durability, and low strength, and thus, the adoption of PLLA implants for the treatment of large orbital wall defects has been limited (KIM et al, 2016).

5) Composites: HA reinforced high-density composite has been used for several years as a bone replacement material. Titanium / PE that uses a thin coating of PE placed on both sides of a titanium mesh minimizes the sharp edges, even when the implant it cut and allows the surgeon to bend and contour a thin implant material to the desired shape.

3.2 COMPUTED TOMOGRAPHY (CT) AND CONE BEAM COMPUTED TOMOGRAPHY (CBCT) TECHNIQUES

In various branches of applied science, there is great interest in reconstructing three-dimensional images from their cross sections, such as medical images, for example computed tomography (CT) is one of the common techniques for capturing information about anatomical details of patients, which are stored as two-dimensional images. The data obtained by these medical imaging systems are usually a set of uniformly spaced parallel slices representing cross-sections of the object under investigation (BERTOL, 2008).

CT imaging remains the gold standard for detecting and defining orbital fractures. Imaging of the entire face is recommended as concomitant fractures are commonly encountered. Coronal and sagittal reconstructions (from axial slice thickness <2 mm), and three-dimensional (3D) rendering is recommended to optimize maxillofacial assessment (BOYETTE et al, 2015).

Recently, preoperative computer-assisted planning using virtual correction models and patient-specific implants using CT mirror images of the non-affected orbit have been introduced. This procedure could reduce operative times and provide more accurate reconstruction on an individual anatomic basis (KIM et al, 2016).

EGGERS et al (2008) compared the geometric accuracy of digital volume tomographic imaging with that of conventional CT and to assess the suitability for image-guided operating. They concluded that the resolution of spatial images was similar for both methods but, however, the spatial accuracy in digital volume tomography was slightly lower than that of CT but still in the sub millimetric range.

According to ABRAMOVITCH & DWIGHT (2014), cone beam imaging technology is most referred to as cone beam computed tomography (CBCT). The terminology "cone beam" refers to the conical shape of the beam that scans the patient in a circular path around the vertical axis of the head, in contrast to the fan-shaped beam and more complex scanning movement of multidetector-row computed tomography (MDCT) commonly used in medical imaging. CBCT is a form of computed tomography (CT). In a single rotation, the region of interest (ROI) is scanned by a cone-shaped x-ray beam around the vertical axis of the patient's head. Digitized information of objects in the ROI such as shape and density are acquired from multiple angles. These imaging data are then processed by specialty software that ultimately constructs tomographic images of the ROI in multiple anatomic planes, namely the standard coronal, axial, and sagittal anatomic planes.

Figure 3: Standard anatomic planes of imaging used for multiplanar reconstructions in cone beam computed tomography (CBCT) and multidetector-row computed tomography.

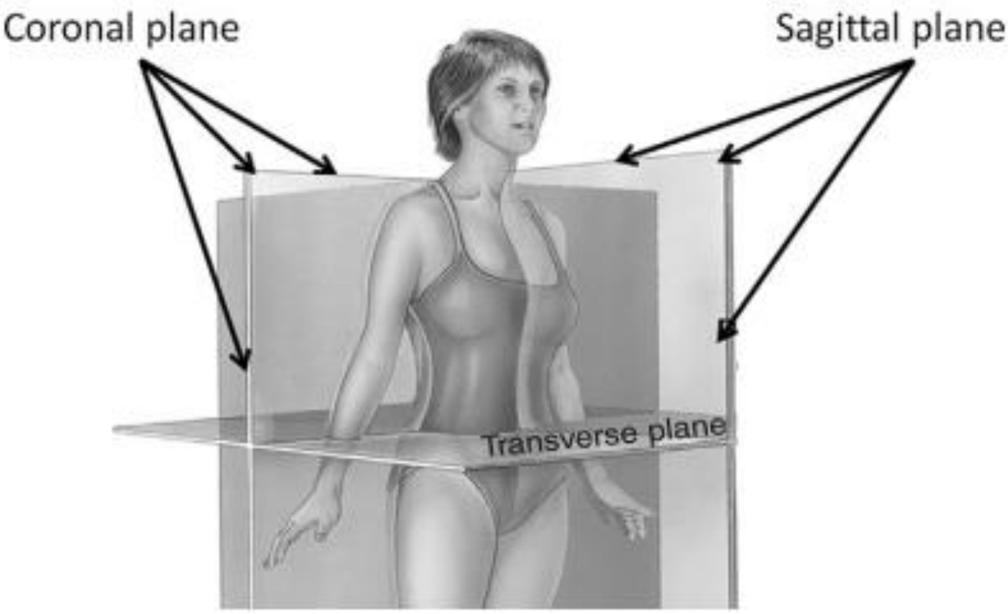

Source: ABRAMOVITCH AND DWIGHT, 2014.

Image reconstruction software programs manage the projection data and construct a 3D volumetric data set. These processed data are then accessed to construct various types of images for display. The choice of images constructed depends on the power of the imaging software and the needs and preferences of the clinician. The image selection from 3D software is not limited to a single type of image display. Depending on the capability of the software, there are multiple options of image construction from the 3D volumetric data set. Most scanner programs display a primary image reconstruction of the object in the 3 anatomic planes of imaging: the axial, sagittal, and coronal planes. They are called primary multiplanar reconstructions and they can be used to construct multiple kinds of secondary reconstructions. The choice of secondary reconstruction is often task specific and is also related to the reconstruction options available on the software. (ABRAMOVITCH AND DWIGHT, 2014).

Nowadays, independent third-part imaging software is commercially available for image reconstruction, which means they are not associated with the capture and proprietary software of the CBCT scanner. If third-party software is being used, the file format of the volume set must be converted from the proprietary file format or file language to a more universal or common digital file format. This common format must be conformant with the Digital Imaging and Communications in Medicine standard (DICOM 09v11dif); that is, the current DICOM standardized file format. This digital format is the International Organization for Standardization (ISO) referenced standardized digital file format for medical images and related information, namely ISO 12052 (ABRAMOVITCH AND DWIGHT, 2014).

3.3 ORBITAL FLOOR FRACTURES MEASUREMENTS AND RECONSTRUCTION

WI et al (2017), evaluated the effect of orbital floor reconstruction and factors related to that in sixty-eight patients with isolated blowout fractures by assessing of orbital volume using orbital CT in cases of orbital wall fracture. The three-dimensional reconstruction technique called Eclipse Treatment Planning System was used to determine the volumes of orbits and herniated orbital tissues. CT was performed preoperatively, immediately after surgery and at final follow ups (minimum six months). They evaluated the reconstructive effect of surgery making a new formula, ‘orbital volume reconstruction rate' from orbital volume differences between fractured and contralateral orbits before surgery, immediately after surgery, and at final follow up.

Before surgery, different tests were performed, including identification of the location and extent of orbital wall fractures and entrapment of extraocular muscle or soft tissue by CT. In each case, bony orbital and herniated orbital tissue areas on sections were measured using a drawing cursor freehand.

Figure 4: Example of orbital volume measurement using 'The Eclipse Treatment Planning System (Ver 13.0, Varian)'. Axial plane: the anterior orbital boundary was defined by a straight line connecting the medial and the lateral orbital rims, and the posterior limit was defined as the orbital apex. Coronal plane: the anterior orbital boundary was defined as the CT slice in which 50% of the inferior orbital rim was visible, and the posterior limit was defined as the orbital apex. Sagittal plane: the anterior orbital boundary was defined by the straight line connecting the superior and inferior orbital rims, and the posterior limit was defined as the orbital apex. The areas of these outlines were measured on each scan and summed to obtain orbital volumes. (a) Preoperative. The red arrow indicates a left inferior wall fracture and herniated orbital tissue before surgery. (b) Postoperative. The green arrow indicates reconstructed left inferior wall fracture. Postoperative image shows reduction of the displaced orbital wall and herniated orbital tissue.

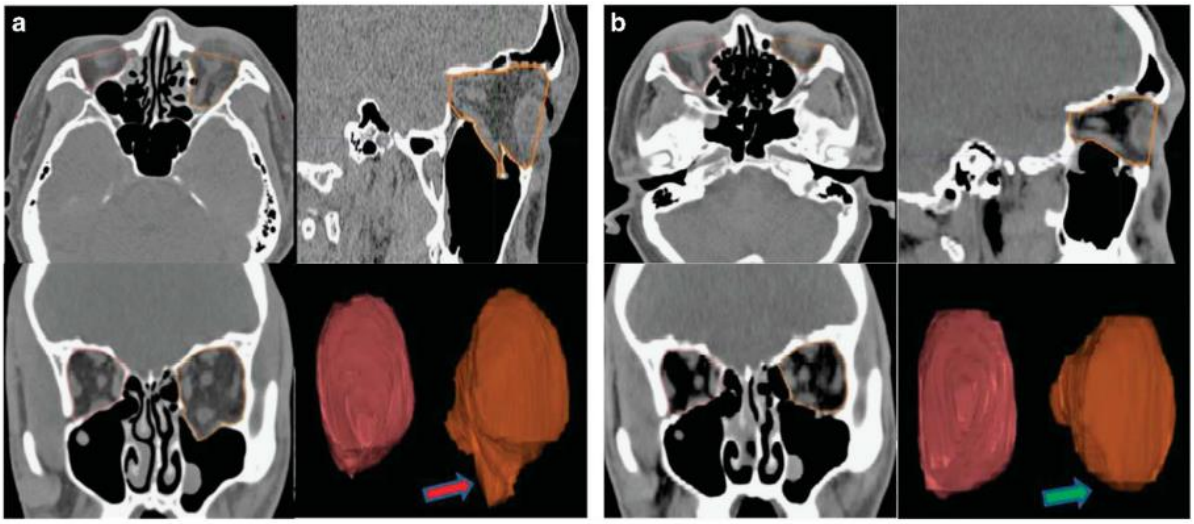

Source: WI et al, 2017.

They obtained then as mean volume of fractured orbits before surgery was 23,01 ± 2,60 cm^3 and that of contralateral orbits was 21,31 ± 2,50 cm^3. The mean orbital volume reconstruction rate obtained was 100,47% immediately after surgery and 99,17% at final follow up. No significant difference in orbital volume reconstruction rate was observed with respect to fracture site or orbital implant type so they conclude that computer-based measurements of orbital fracture volume can be used to evaluate the reconstructive effect of orbital implants and provide useful quantitative information.

GANDER et al (2014) did a new approach using individually manufactured titanium implants (KLS Martin Group, Tuttlingen, Germany) for daily routine by processing preoperative CT-scan data to generate a 3D-reconstruction of the affected orbit using the mirrored non-affected orbit as template and the extent of the patient specific implant (PSI) was outlined, three landmarks were positioned on the planned implant to allow easy control of the implant's position by intraoperative navigation. PSI allows precise reconstruction of orbital fractures by using a complete digital workflow and should be considered superior to manually bent titanium mesh implants.

VEHMEIJER et al (2016) studied a simple, precise, cost-effective method of treating orbital fractures using 3D printing technologies in combination with autologous bone. The study was performed in a 64-year-old female patient with enophthalmos, and diplopia developed due to an orbital floor fracture. A virtual 3D model of the fracture site was generated from computed tomography images of the patient. The fracture was virtually closed using spline interpolation. Furthermore, a virtual individualized mold of the defect site was created, which was manufactured using an inkjet printer. The CT slices resulted in DICOM file that were imported to a software and then a 3D model of the patient’s skull was created.

Figure 5: CT image from coronal view showing a blowout fracture of the left orbit with protruding soft tissue into the maxillary sinus.

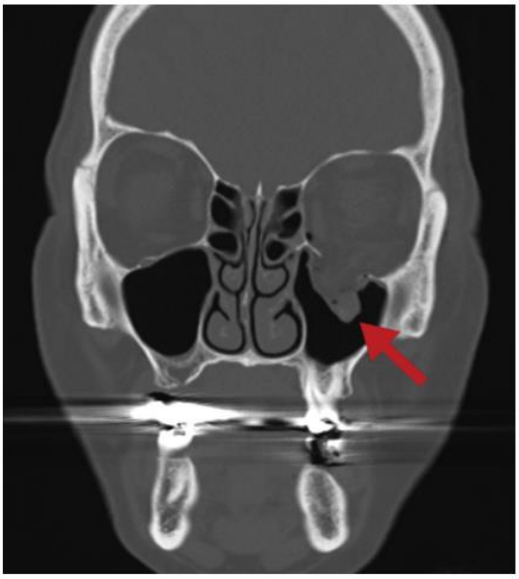

Source: VEHMEIJER et al, 2016.

The virtual 3D model was used to manufacture a 3D printed mold of the virtually reconstructed orbital floor and they were virtually drawn through the defect site to reconstruct the missing orbital floor bone.

Figure 6: Virtual 3-dimensional model of the patient's skull (gray part); virtual mold of the orbital floor (A); virtually reconstructed bone defect (B); and the spline interpolation curves (C).

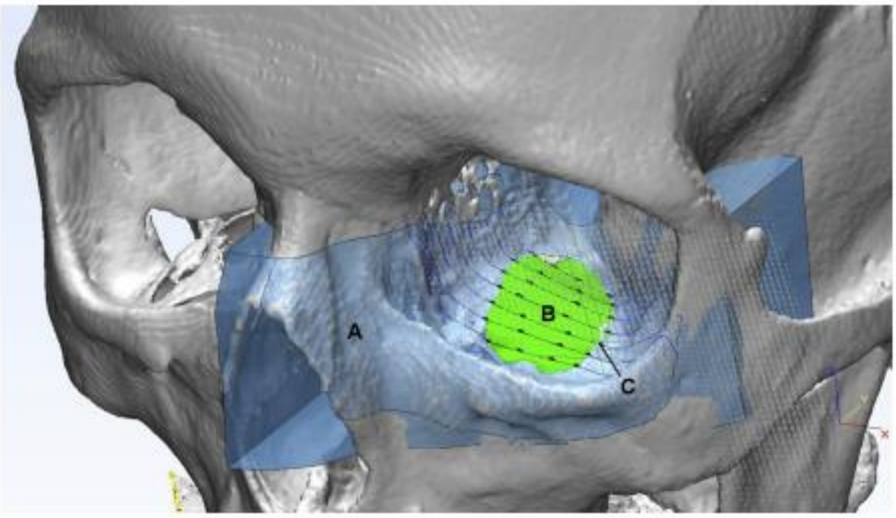

Source: VEHMEIJER et al, 2016.

MANCHIO et al (2010) studied the role of sagittal reformatted computed tomographic images in the evaluation of orbital floor fractures. They measured maximum fracture width, depth, posterior shelf length (PSL), where the direct fracture width measurements were obtained via coronal images, whereas depth and PSL were measured directly in the sagittal plane. Indirect measurements in a given plane were obtained by counting the number of slices in which the fracture was present and multiplying by the slice thickness.

ANG et al (2015) designed a protocol for CT measurement of orbital floor fractures using computer software by 15 independent observers without clinical experience in orbital fracture detection. If surgery is indicated, orbital floor size measurements from CT scans can determine the dimensions of orbital implants used for surgery, which can affect postoperative outcomes.

The software used to operate was a free Digital Imaging and Communications in Medicine (DICOM) viewer software program—OsiriX v4.1.2 (Pixmeo, Geneva, Switzerland). Their analysis assumes that the orbital floor is a plane structure when calculating the surface area, although in the reality the orbital floor is a 3D structure with contours. The protocol was divided in qualitative and quantitative aspects as follows:

1) Qualitative aspects included identifying:

   - Direct signs of orbital fractures: abrupt changes in bone density or bone thickness, interruption of cortical bone continuity, abnormal angulation between bones and displaced bone fragments.

   - Indirect signs of orbital fractures: opacification of adjacent paranasal sinuses, presence of air-fluid levels in the sinuses, intraorbital and periorbital subcutaneous emphysema, surrounding soft tissue edema.

Figure 7: Direct signs of orbital floor fractures. (a) Right orbital floor fracture with an abrupt change in bone density. (b) Right orbital floor fracture with an interruption of cortical bone continuity. (c) Abnormal angulation between the right orbital floor and a displaced bone fragment.

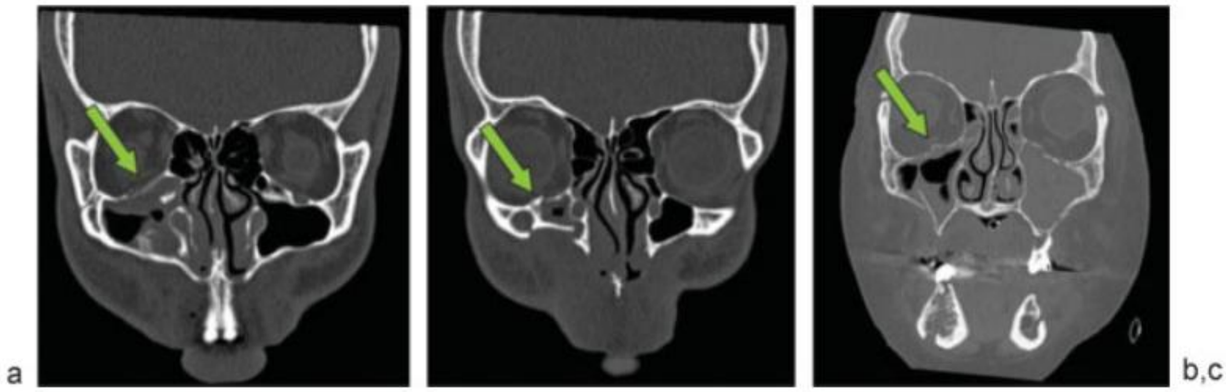

Source: ANG et al, 2015.

Figure 8: Indirect signs of orbital fractures. (a) Coronal view of a left orbital floor fracture with opacification of the left maxillary sinus. (b) Presence of an air-fluid level in the right sphenoid sinus. (c) Intraorbital and periorbital subcutaneous emphysema in a bilateral orbital fracture. (d) Surrounding soft tissue edema in a patient with multiple facial fractures.

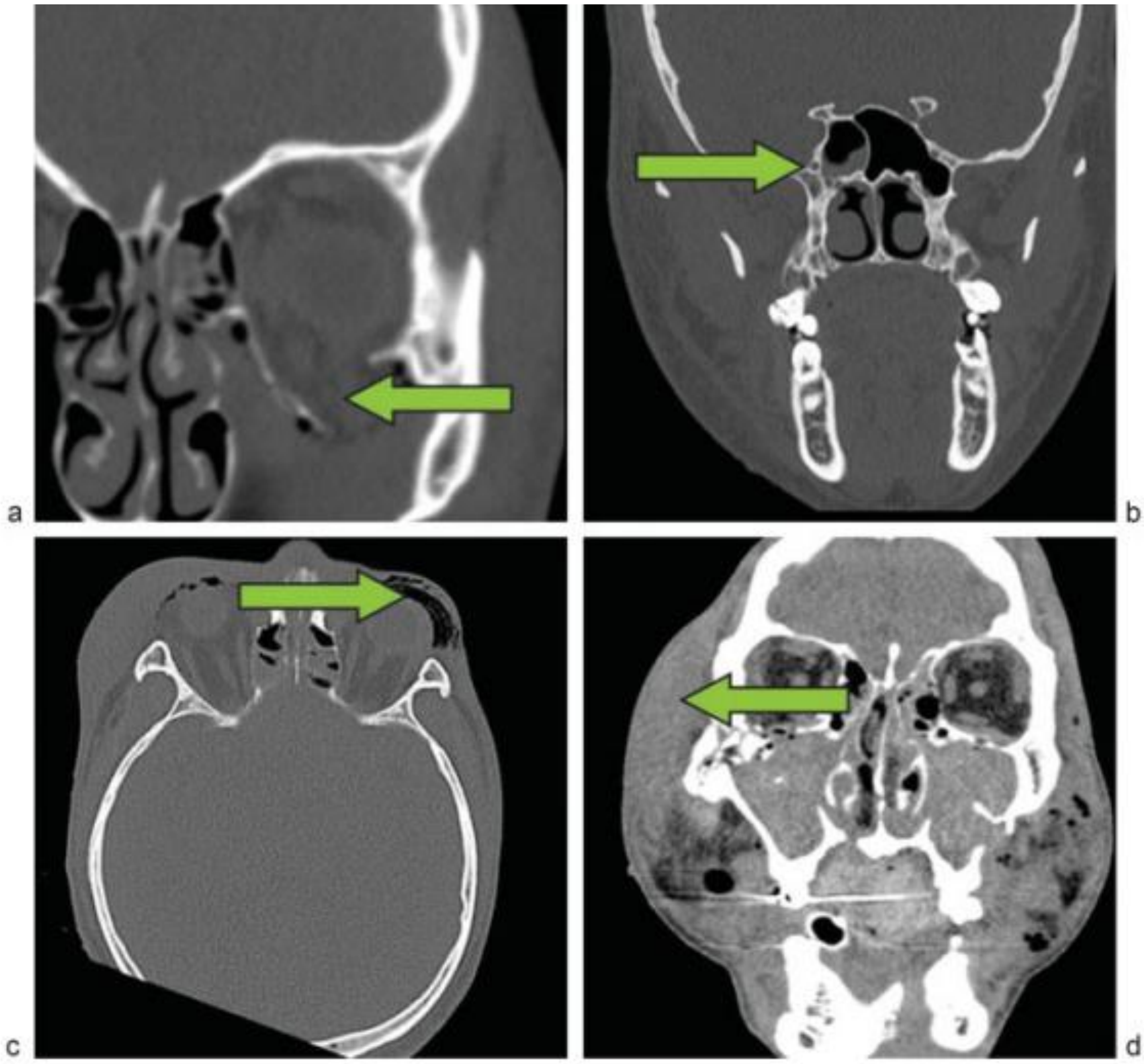

Source: ANG et al, 2015.

2) Quantitative aspects: identification of orbital floors defects using the normal limits of the orbital floor in the coronal (frontal) sections, placement of points of interest at the superior aspects of the fracture limits in all coronal sections, reconstruction of the axial images, making out the edges of the fracture and finally connecting all the previously placed points of interest and measuring the area bounded by them to get the surface area of the defect.

Figure 9: Limits of orbital floor.

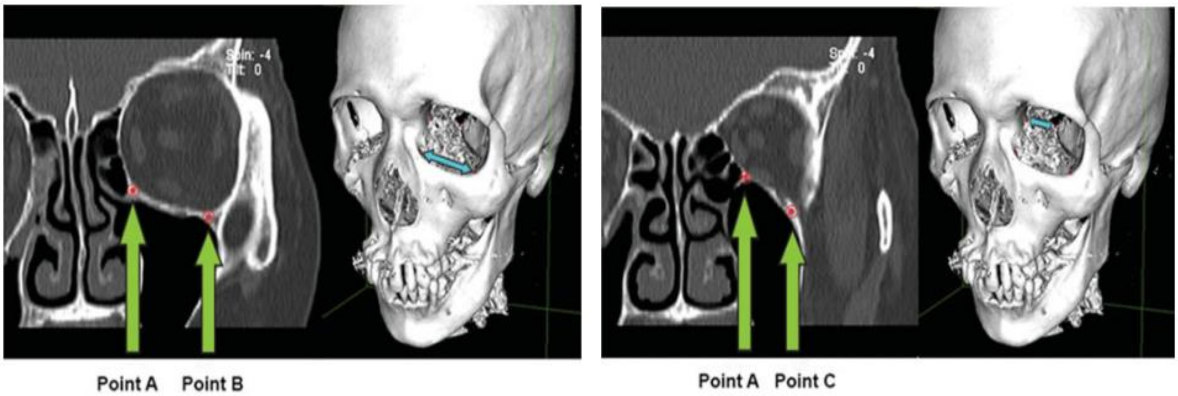

Source: ANG et al, 2015.

Figure 10: Creating the surface area or orbital floor defect. First, by marking out the edges of the fracture. (a) Left orbital floor fracture with fracture size measured from the superior aspects of the fracture limits. (b) Stacking the reconstructed axial views onto each other by increasing the slab thickness, to view all the points of interest in a single layer. (c) Magnifying the area bounded by the points of interest by zooming in such that it fits the entire screen, to get a more accurate measurement by considering any irregular edges. Second, by connecting the previously placed points of interest and measuring the area bounded by them to get the surface area of the defect. And finally, by connecting all the points of interests allows the surface area of the orbital floor fracture to be measured.

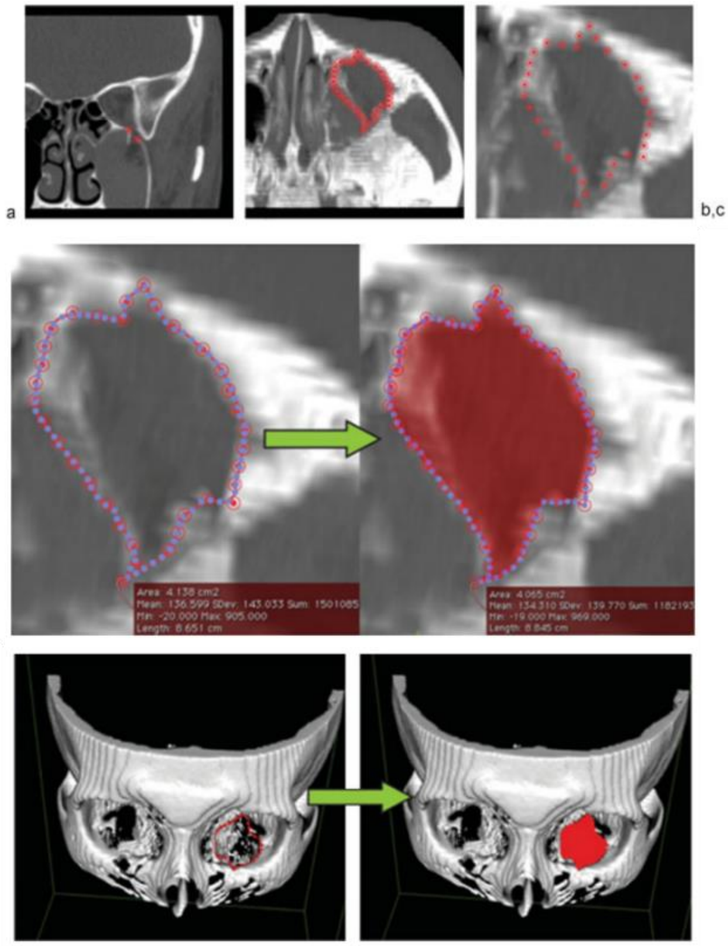

Source: ANG et al, 2015.

The values that were obtained by them for the orbital floor fractures using this method are presented on the table below:

Table I: Measurement of orbital floor defects.

MEASUREMENT	SURFACE AREA OF OFBITAL FLOOR FRACTURE (mm^2)
Patient A	121,80 – 199,00
Patient B	334,80 – 424,90
Patient C	384,10 – 461,90

Source: Adapted from ANG et al, 2015.

They concluded that their novel protocol in CT measurements of orbital fractures is easy to teach and utilize, and can be applied in clinical situations easily, and it can assist a novice reader in detecting an orbital floor fracture and quantifying it easily with a low degree of interobserver variability. Also, they point out that the disadvantage associated with all of the earlier methods is that the surface of the defect is extrapolated from a few linear measurements rather than from the precise measurement of the entire area of the defect.

4 MATERIALS AND METHOD

For the measurements, the protocol from ANG et al (2015) was used as guide for the present work. The software chosen for the analysis of orbital floor fractures imaging data was VGSTUDIO MAX (Volume Graphics GmbH, Heidelberg, Germany). To be able to perform the measurements properly on the software chosen, a study of it and its parameters were conducted so all the results obtained were the same.

4.1 PATIENT DATA

In this study, the datasets used were real CT datasets resulting from routine diagnostics. All imaging data were kindly provided by Charité – University Hospital Berlin and were available in anonymized format. A valid vote of the local ethics committee has been obtained for the use of the data (EK 392082019). The datasets were obtained from 12 anonymous patients, and they were all DICOM image stack files.

4.2 VGSTUDIO MAX SOFTWARE

A test license of the VGSTUDIO MAX software was used for this bachelor thesis (VGSTUDIO MAX 3.4 evaluation license). VGSTUDIO MAX is a choice for visual quality inspection in industrial applications and for the visualization of data in fields of academic research. It covers the entire workflow, from the precise reconstruction of three-dimensional volume data sets using the images taken by CT scanner to visualization (in 3D and 2D) and the creation of animations. The software can calculate 3D volume data sets from the images taken by a CT scanner, which can then be analyzed and visualized on it.

This was the first time that VGSTUDIO was used for CT and DVT imaging data analysis of patients with orbital floor defects, so some parameters need to be studied and defined before starting the analysis. To obtain this information, the following tutorials provided by Volume Graphics (VG) were studied:

- First Steps;
- Loading Data in VGSTUDIO MAX;
- Surface Determination;
- Segmentation;

- Coordinate Measurement;

- Rendering a Volume Object;

- CT Reconstruction.

4.2.1 PARAMETERS

The DICOM files were imported in VGSTUDIO MAX from a chosen directory. The CT and DVT scans are formed by several slices of images that together allow us to see all parts of the area of interest in different 3D positions. Parameters were set for loading the DICOM files and for preparing the generated 3D image for the measurements analyze. They are explained as follows.

4.2.1.1 Loading parameters

The parameters used for loading the DICOM image stack files on VGSTUDIO MAX are well-marked on the image below:

Figure 11: Parameters used for settings when loading the DICOM image stack on VGSTUDIO MAX.

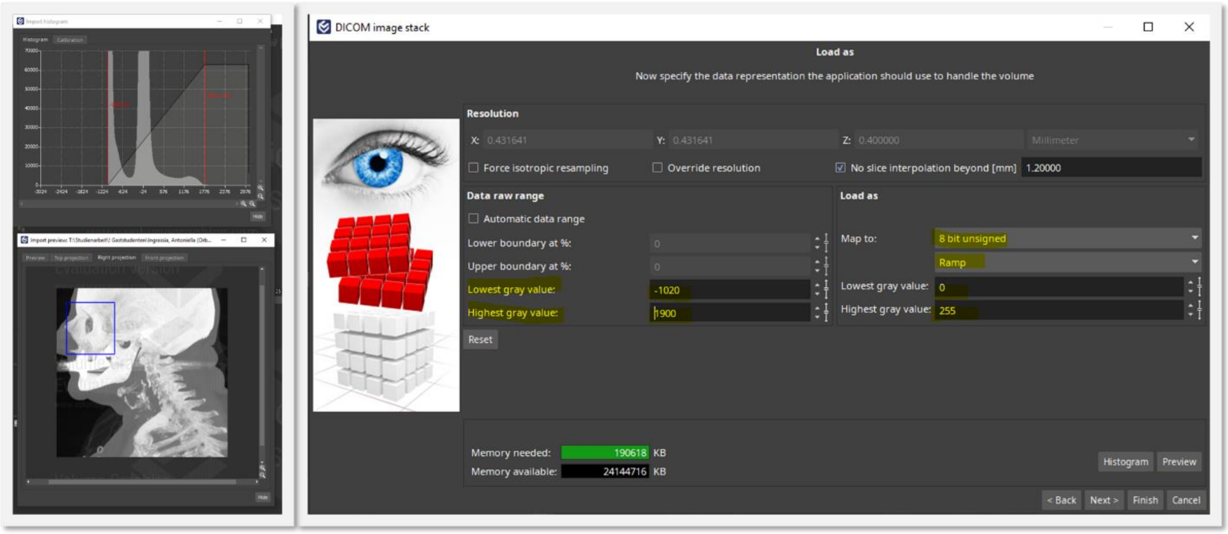

Source: the author, 2021.

- <u>Histogram:</u> it shows the gray value distribution of the data set. On the left, there is the air peak, and in the middle and on the right, there are two material peaks. The better the peaks are separated, the stronger the contrasts in the visual representation in the 2D windows;

- Grey Values: To restrict the gray value range to the relevant data, it is possible to click and drag the red lines on the left and right of the histogram to the lowest gray value (before the air peak) and to the highest gray value (after the material peak), respectively. For the CT/CBCT images analyzed here the values used were -1020 for the lowest and 1900 for the higher. All gray values will be loaded, but the parts of the data set that do not contain any (relevant) gray values will be mapped to the lowest and the highest gray value, respectively;
- Resolution: it is important to pay attention to the values of the resolution on x, y and z and if they match the original data sets, otherwise the 3D image formed will be distorted, and then all the calculations will not be correct;
- 8 bit unsigned: to reduce the amount of data to be loaded;
- Ramp: it is the default setting, the gray values below the lower limit will be set to the value of the lower limit, and the gray values above the upper limit will be set to the value of the upper limit. The gray values within the gray value range will be imported with their original gray values;
- Preview: it shows a slice preview of the object corresponding to the gray value range specified in the import histogram. On the projection tabs, it is possible to drag the blue lines to reduce unnecessary surrounding air and areas by specifying a region of interest. In the case of the CT/DVT images, the important area is around the eye, where there is the orbital floor.

4.2.1.2 Pre-measurements parameters

After finalizing the loading parameters, the files are completely imported, and the project is ready to be initiated. By default, the 2D and 3D images generated by the software are as follows:

Figure 12: Images generated by default by VGSTUDIO MAX.

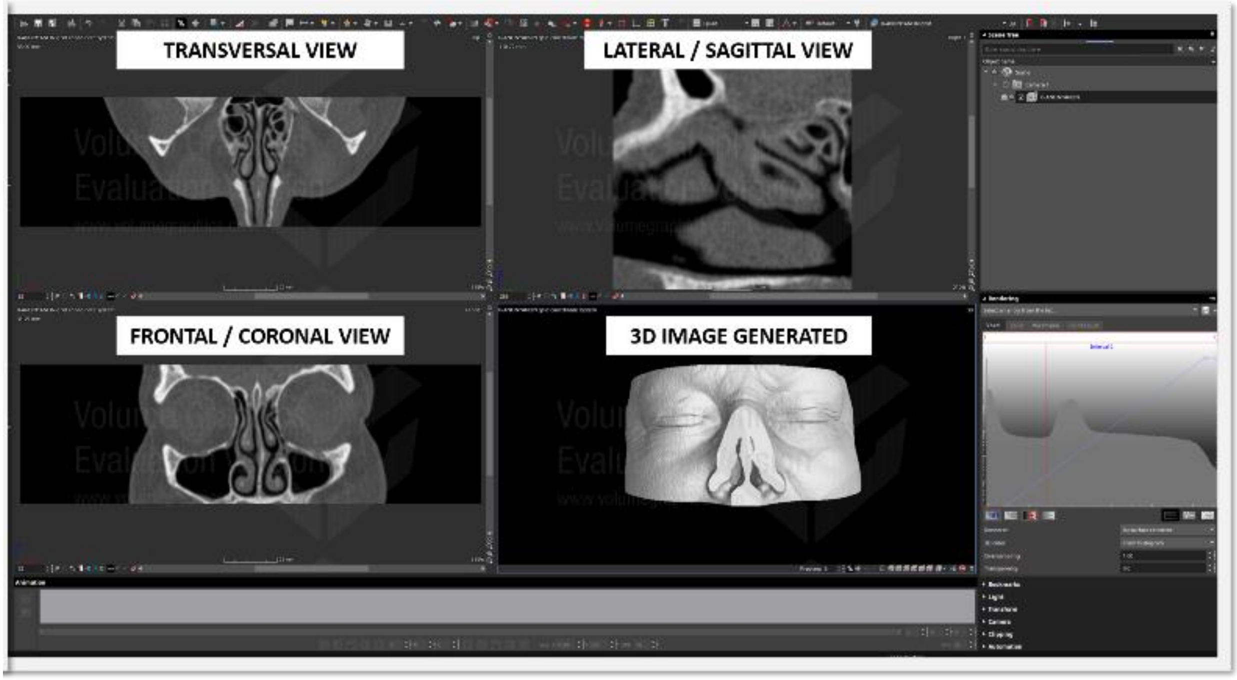

Source: the author, 2021.

The 3D image generated considers all the types of tissues, from bone to air. To be able to delimit the analysis only in the bone tissue part, it is necessary to segment the tissues into different Regions of Interest (ROI's) using grey value ranges. The table below shows the values for each type of tissue.

Table II: Grey values determined for each type of tissue.

TYPE OF TISSUE	LOWEST GREY VALUE	HIGHEST GREY VALUE
BONE	105,00	250,00
SOFT	65,00	104.90
AIR	0,00	65,00

Source: the author, 2021.

The 3D image will appear after this change as in the figure below.

Figure 13: 3D image with grey values for bone tissue.

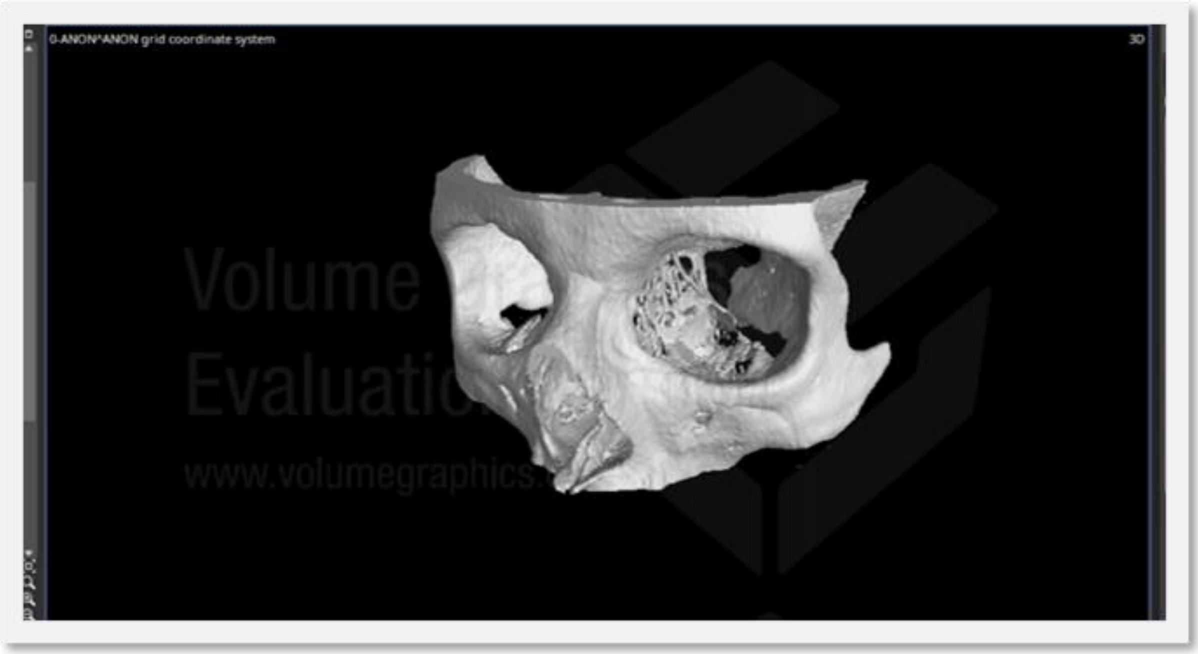

Source: the author, 2021.

- <u>Surface determination</u>: determines the boundary between background and material through the surface of a volume object by defining the grey values.

Two types of surface determination can be applied:

1) <u>Isovalue-based Surface Determination</u>: the result is a material boundary defined by one gray value that is globally applied to the data set. This surface is referred to as the isosurface. In the histogram, the gray value of the surface is marked by a red vertical line, the isovalue line. This gray value serves as a threshold: Brighter areas are considered material, while darker areas are considered background.

2) <u>Advanced Surface Determination</u>: adapts a starting contour (e.g., the isosurface, an ROI, a CAD model, or a surface mesh) based on the local gray value gradients.

To be more accurate, the surface determination used was the advanced one. The parameters set for this are shown below:

Figure 14: Advanced surface determination parameters.

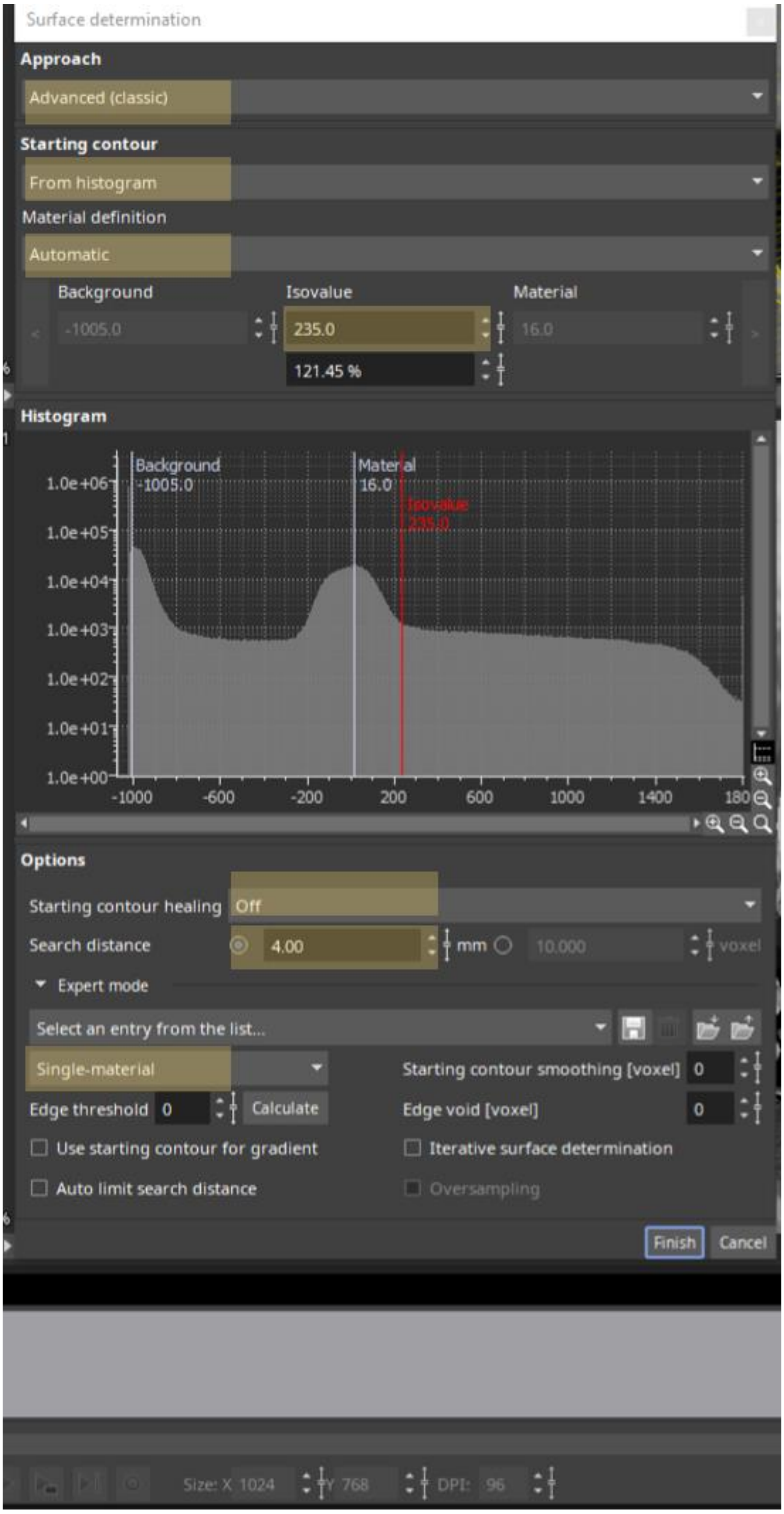

Source: the author, 2021.

- Approach: Advanced (classic);
- Material definition: automatic;
- Isovalue: 105 (the lowest grey value for bone tissue);
- Starting contour healing: off;
- Search distance value: 4 (indicated).

In the 2D windows, a faint yellow line will show the starting contour, the hairlines along the starting contour will show the search direction for the local gray value gradients, and a stronger yellow line will show a preview of the surface (figure below).

Figure 15: Preview of the surface on 2D images.

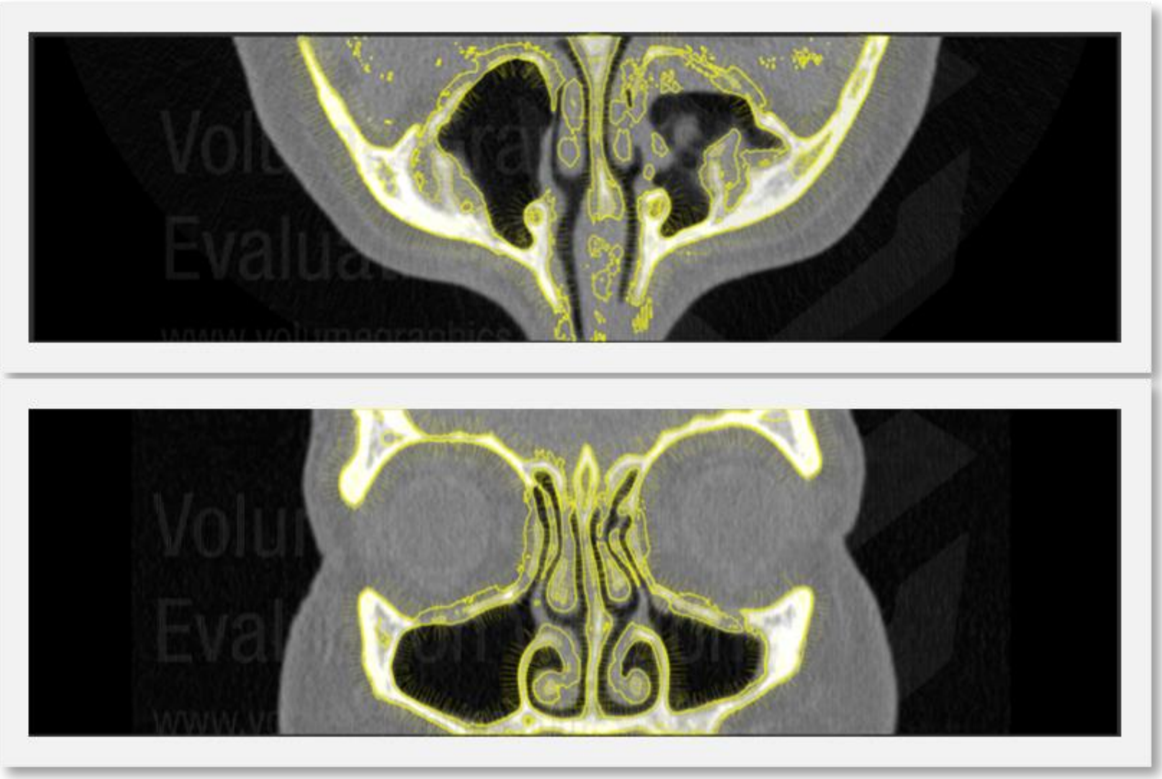

Source: the author, 2021.

Now that all the parameters are set, the measurements can be done properly.

4.3 MEASUREMENTS

Before beginning the measurements, an overview of all patients was done to do the qualitative analysis of the CT/CBCT views and to know which side was with an orbital floor defect. The images were first analyzed on a free software called Stratovan

Pro Surgical 3D (Vers. 2021.04.21.0719, Stratovan Corp, Davis, CA, USA), used for 3D DICOM Viewer for surgeons and patient education. The table below presents all the preview information obtained before loading the data sets into VGSTUDIO MAX: patient ID, diagnosis of orbital floor fracture (OBF), the side of the defect, modality, number of slices and resolution.

Table III: Overview of patient's data before loading on VGSTUDIOMAX.

PATIENT ID	DIAGNOSIS / DEFECT SIDE	MODALITY / NUMBER OF SLICES	RESOLUTION IN X Y Z [mm]
Orbital_001	OBF / BOTH SIDES	DVT / 433,00	0,40 0,40 0,40
Orbital_002	OBF / LEFT SIDE	CT / 543,00	0,43 0,43 0,40
Orbital_003	OBF / RIGHT SIDE	DVT / 433,00	0,40, 0,40 0,40
Orbital_004	OBF / RIGHT SIDE	CT/ 285,00	0,36 0,36 0,63
Orbital_005	OBF / LEFT SIDE	CT / 73,00	0,32 2,72 0,32
Orbital_006	OBF / LEFT SIDE	CT / 186,00	0,38 1,00 0,38
Orbital_007	OBF / RIGHT SIDE	CT / 321,00	0,47 0,47 0,63
Orbital_008	OBF / LEFT SIDE	CT / 319,00	0,47 0,47 0,63
Orbital_009	OBF / RIGHT SIDE	DVT / 575,00	0,40 0,40 0,40
Orbital_010	OBF / RIGHT SIDE	CT / 130,00	0,44 0,44 1,50
Orbital_011	OBF / LEFT SIDE	CT / 377,00	0,30 0,30 0,40
Orbital_012	OBF / LEFT SIDE	CT / 191,00	0,48 0,48 1,50

Source: the author, 2021.

The CT/DVT images analyzed for finding out the diagnosis are presented on figures 13, 14 and 15 below. The qualitative part of the method used by ANG et al (2015), and some literature papers already mentioned before were used for searching direct and indirect signs of orbital fracture. Usually there will be a difference of level between normal and broken side, along with the presence of broken bones (lack of continuity) and the presence of soft tissue on the sinus area. Moreover, the most common view used for doctors to identify a defect is the coronal one.

Figure 16: CT and CBCT/DVT slice images generated by PRO SURGICAL 3D software for patients 001 to 004. Patients 001 and 003 examined in CBCT/DVT modality and patients 002 and 004 in CT modality.

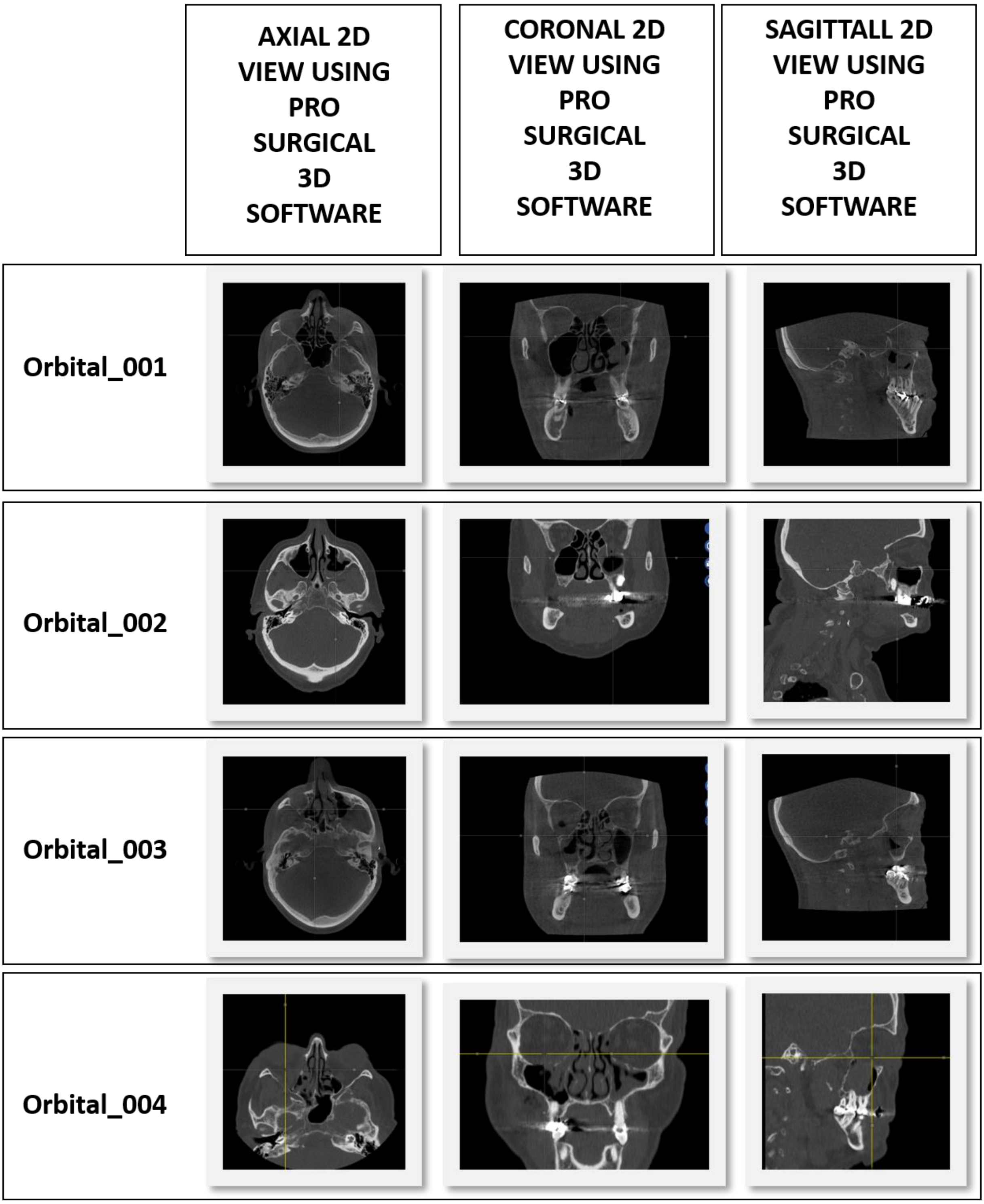

Source: the author, 2021.

Figure 17: CT slice images generated by PRO SURGICAL 3D software for patients 005 to 008. All patients examined in CT modality.

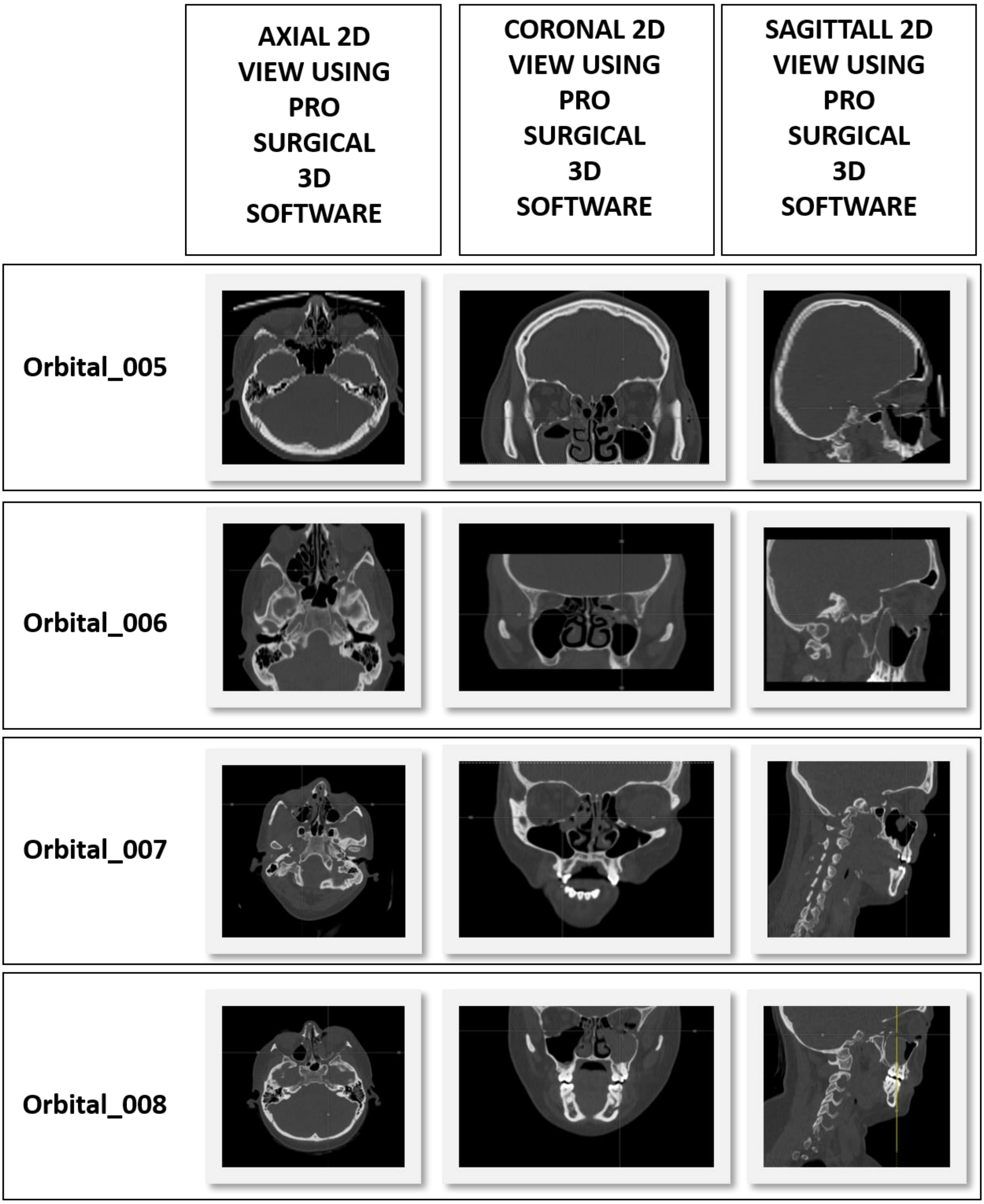

Source: the author, 2021.

Figure 18: CT and DVT slice images generated by PRO SURGICAL 3D software for patients 009 to 012. Patient 009 examined in CBCT/DVT modality and patients 010, 011 and 012 examined in CT modality.

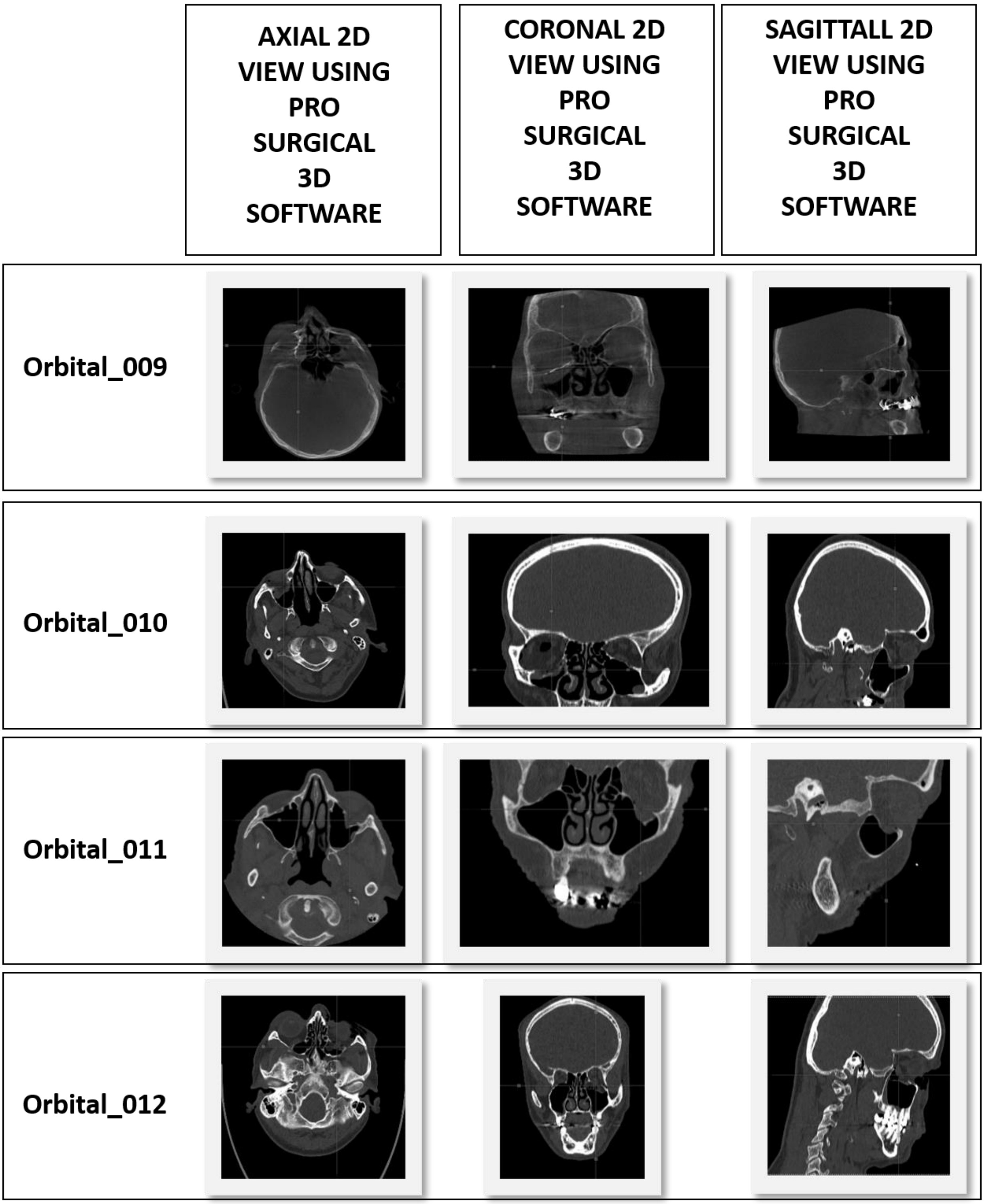

Source: the author, 2021.

For the quantitative part, the measurements of interest were:

- Length and depth of total orbital floor using coronal and sagittal views;

- Length and depth of the defect on the orbital floor using coronal and sagittal views;
- Surface area of total orbital floor;
- Surface area of the defect on the orbital floor;
- Maximum length and depth of the defect using the surface area already obtained before.

Two tools of VGSTUDIO MAX were used for these measurements, distance instrument and polyline draw to make the surface area.

Figure 19: VGSTUDIO MAX tools for the measurements.

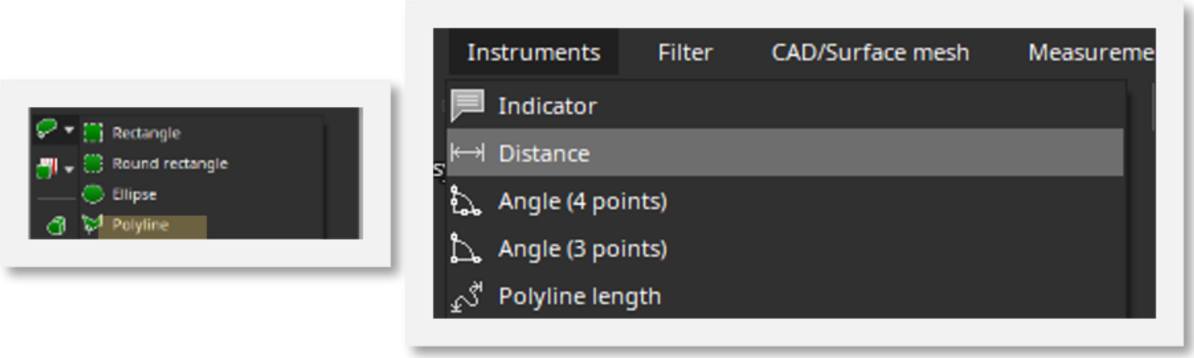

Source: the author, 2021.

For the measurements of total orbital floor using coronal and sagittal views, the lower and the upper limit of orbital floor were defined first.

Figure 20: Upper and lower limits of orbital floor using coronal view.

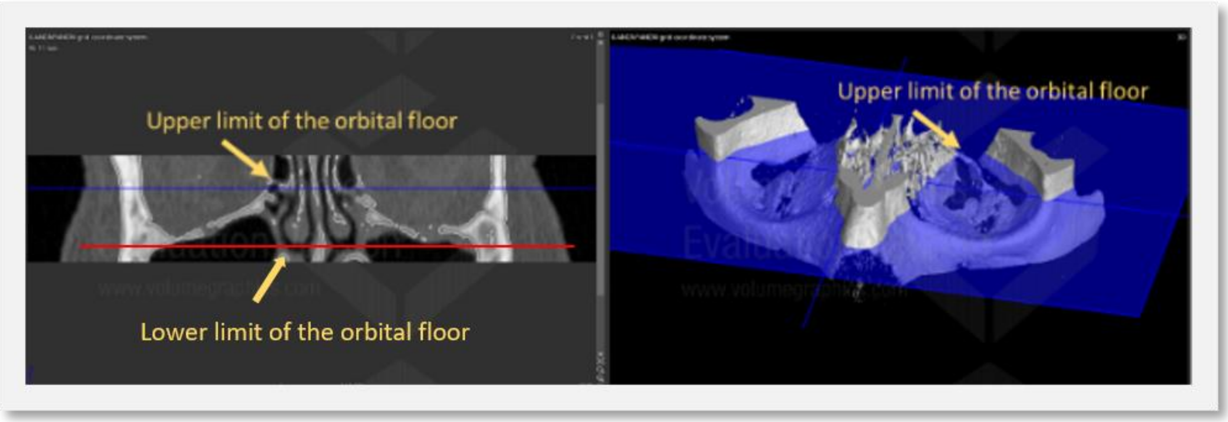

Source: the author, 2021.

4.4 STATISTICAL ANALYSIS

Mean values and standard deviation (SD) were calculated using Excel software for Windows, version 2109. Mean differences of a continuous variable between 2 groups were tested with Student's unpaired *t* test using GraphPad Software, 2021 online version. All *P* values are 2-tailed with significance level at $P < 0,05$ – which means that if $P \geq 0,05$ then the results differences are considered to be not statistically significant, showing reproducible results.

5 RESULTS AND DISCUSSION

The measurements were performed using VGSTUDIO MAX, and the analysis of orbital floor blowout fractures using anonymized CT/DVT scans were done as follows:

5.1 ASSESSMENT OF TOTAL ORBITAL FLOOR AND ORBITAL FLOOR FRACTURES

For the analysis not just the orbital floor defect was measured but also the total orbital floor area was measured to compare them in surface area unit. First, depth, length and surface area were measured for the total orbital floor – both sides, then depth, length, and surface area were measured for the orbital floor defect.

5.1.1 Analysis of total orbital floor – depth, length, and surface area

The measurements of depth and length of total orbital floors are presented on the image below for one anonymized patient as example. The measurements of depth were made using the 2D sagittal view based on the limits pre-defined before. The measurements of length were made using the 2D coronal view also based on the limits of orbital floor pre-defined before. Both measurements were done using the distance instrument tool of VG STUDIO MAX.

Figure 21: Representation of measurements of depth and length made for total orbital floor areas using coronal and sagittal views on VGSTUDIO MAX - patient Orbital-002. Red arrow shows depth measurements and blue arrow shows length measurements, and in which direction they appear on each screen of the software. The green lines are the ones measured on the software. Solid arrows are the ones placed on the exact CT slice of the images; dot arrows are the ones place in different CT slices.

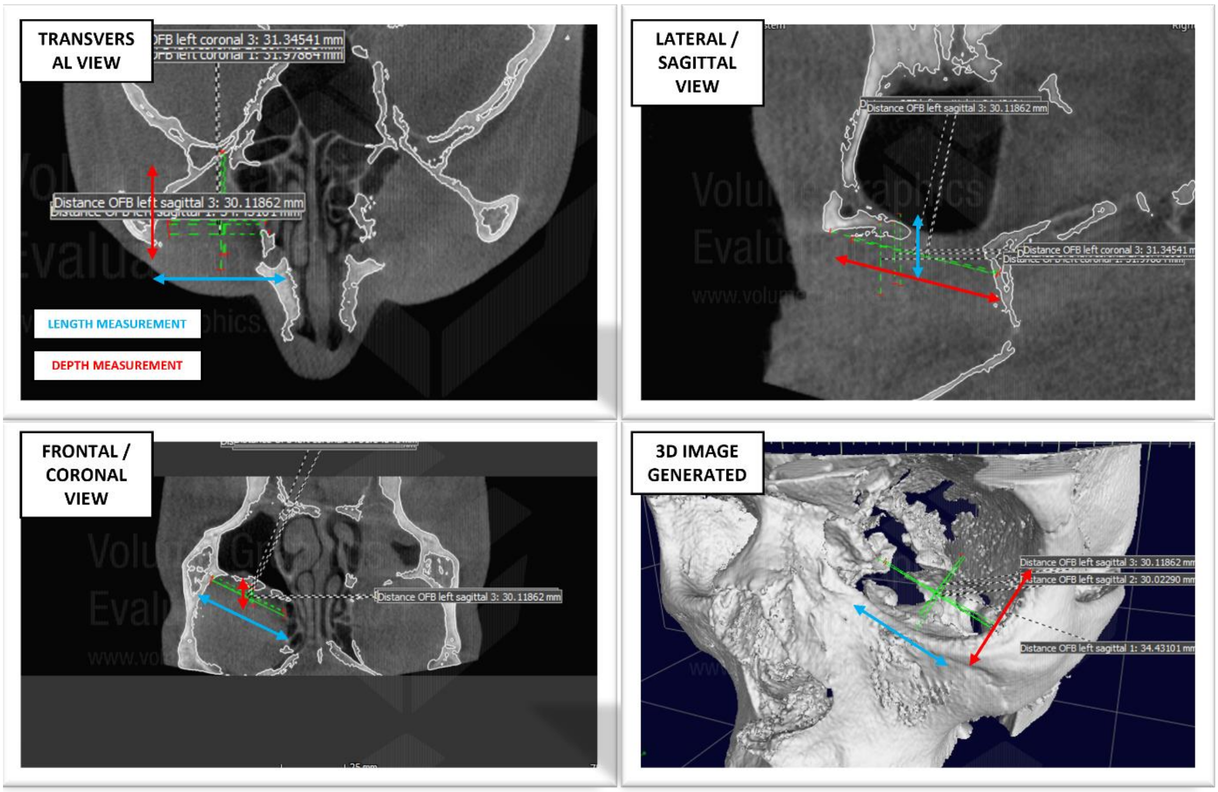

Source: the author, 2021.

All the measurements were done three times for statistical results and the all the tables show the range for the values obtained in each one. All the tables also present the side of orbital floor that has a fracture. The measurements of depth and length of total orbital floor for both sides are presented on the table below.

Table IV: Result of measurements range of depth and length of total orbital floor areas using coronal and sagittal view on VGSTUDIO MAX.

PATIENT ID	DEFECT SIDE	ORBITAL FLOOR LEFT SIDE		ORBITAL FLOOR RIGHT SIDE	
		LENGTH [mm]	DEPTH [mm]	LENGTH [mm]	DEPTH [mm]
Orbital_001	BOTH	30,44 - 31,98	30,02 – 34,43	27,20 – 28,35	25,16 – 27,18
Orbital_002	LEFT	23,59 – 26,51	30,09 – 32,25	25,07 – 25,71	34,10 – 35,48
Orbital_003	RIGHT	26,33 – 30,40	31,09 – 40,60	29,37 – 31,48	28,75 – 33,31
Orbital_004	RIGHT	25,52 – 27,70	27,80 – 31,12	24,95 – 27,59	29,10 – 31,64
Orbital_005	LEFT	31,44 – 33,66	27,17 – 28,63	27,88 – 31,25	30,85 – 33,52
Orbital_006	LEFT	28,52 – 29,94	27,85 – 32,02	22,42 – 23,32	27,04 – 29,66
Orbital_007	RIGHT	24,09 – 26,01	24,54 – 25,80	23,68 – 27,78	27,86 – 33,08
Orbital_008	LEFT	23,37 – 26,51	25,67 – 28,54	26,81 – 28,40	26,52 – 33,04
Orbital_009	RIGHT	27,72 – 29,53	29,04 – 29,75	31,04 – 32,62	27,91 – 30,34
Orbital_010	RIGHT	27,89 – 28,88	30,71 – 30,85	24,73 – 28,16	22,62 – 27,09
Orbital_011	LEFT	24,14 – 25,44	23,73-31,11	27,51 – 28,66	24,98 – 25,40
Orbital_012	LEFT	32,13 – 33,33	31,26 – 32,21	31,62 – 32,30	30,78 – 33,11

Source: the author, 2021.

ANG et al (2015) used on their protocol the coronal slices to place points on the fracture limits and after connected all of them creating then a plane surface. On

VGSTUDIO MAX it is not possible to do the same because the software does not allow the user to go through different coronal slices to place the points, it is only possible to it in the same slice all together. To overcame this, the transverse view was used to place the points with the polyline tool so we would have a parallel surface to the orbital floor, just like on the protocol used as guide. The coronal view was still necessary as guide to see where the limit parts of the total orbital floor and the limits of the defect were itself. The total surface areas obtained are presented on the image following:

Figure 22: Total orbital floor surface area drawing on VGSTUDIO MAX using polyline tool – Patient Orbital – 001.

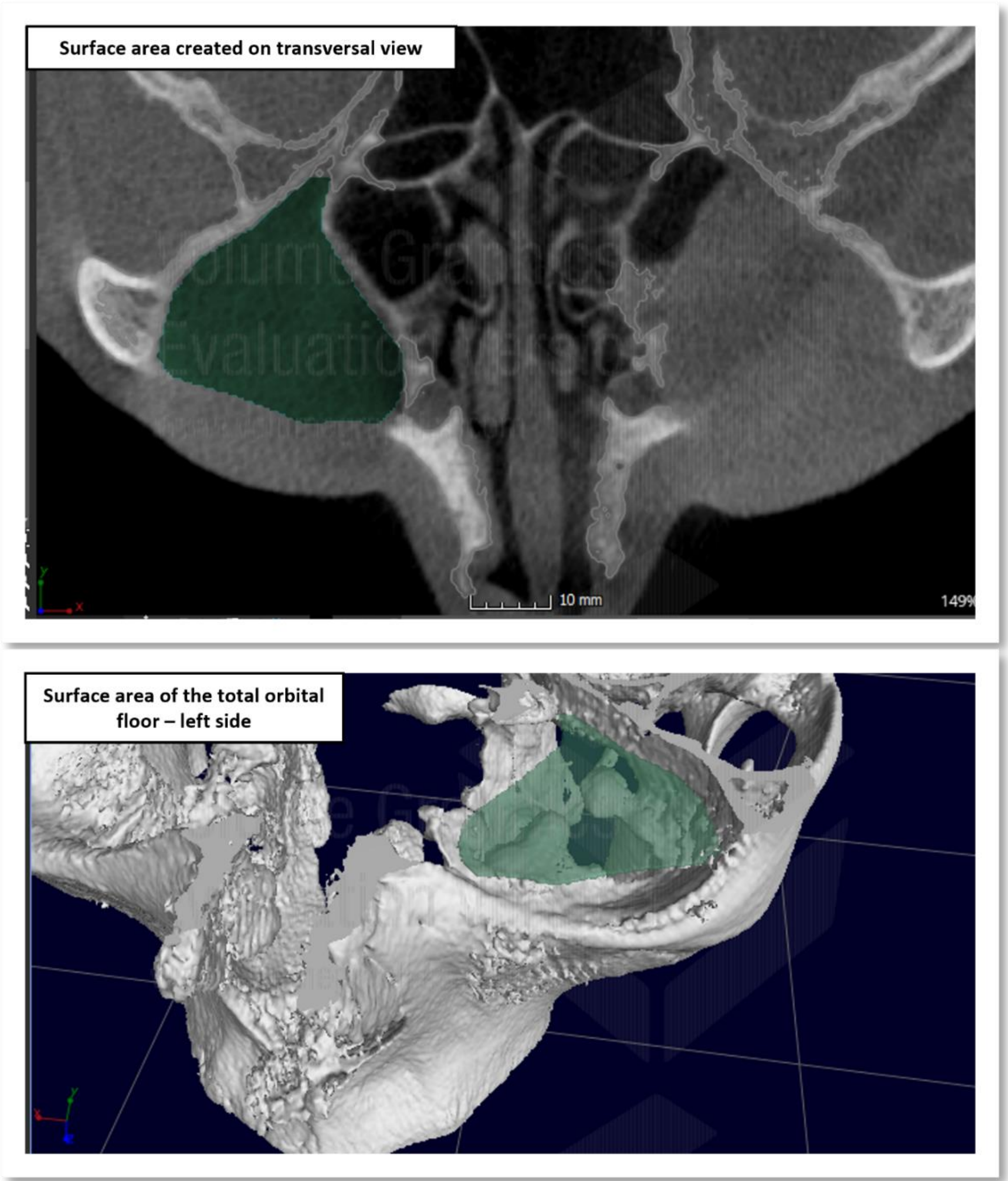

Source: the author, 2021.

To create the surface area, it is mandatory to use de transversal 2D view to place de points. They will connect on each other so a yellow area will appear representing the surface area and this will be the new ROI. Since this area does not have bone, and the parameters are set to bone tissue, it is necessary to change the isovalue to zero so the software will consider the area as a solid part.

Figure 23: Points placed on the transversal view, generating a yellow area that will become the new ROI, hence the surface area.

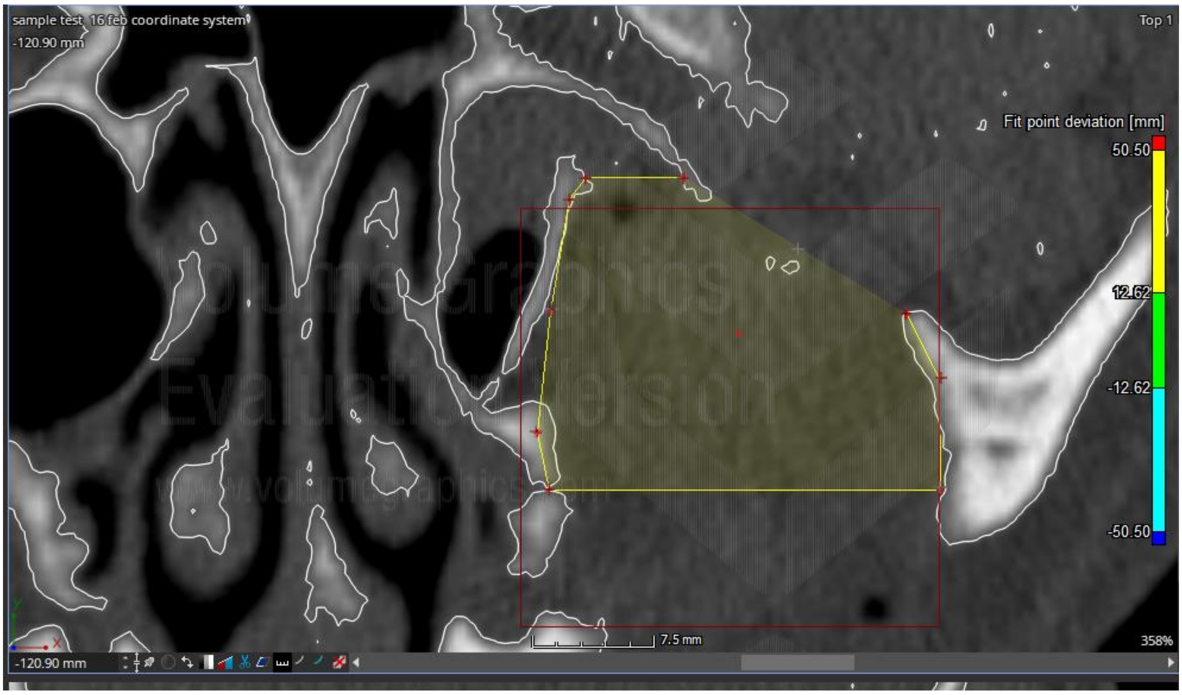

Source: the author, 2021.

The value of the orbital floor surface area is obtained directly from the software once the surface area is made. The only action that needs to be done is to divide the value provided by two because the software considers both sides of the surface created (up and down). The lateral surface is minimum since the thickness of the surface created is minimal, therefore this portion can be disregarded on the result. The results of total surface area measurements are presented on table V.

Table V: Results of the measurements range of total orbital floor surface areas using transversal view.

PATIENT ID	DEFECT SIDE	ORBITAL FLOOR TOTAL SURFACE AREA	
		LEFT ORBITAL [mm²]	RIGHT ORBITAL [mm²]
Orbital_001	BOTH	561,06 – 660,71	630,81 – 699,80
Orbital_002	LEFT	462,69 – 528,14	328,19 – 489,10
Orbital_003	RIGHT	665,58 – 860,47	657,63 – 799,98
Orbital_004	RIGHT	366,87 – 548,45	325,22 – 362,98
Orbital_005	LEFT	675,59 – 775,30	637,98 – 876,23
Orbital_006	LEFT	493,16 – 569,30	672,97 – 720,01
Orbital_007	RIGHT	443,15 – 465,68	446,95 – 504,13
Orbital_008	LEFT	731,19 – 815,52	746,84 – 969,57
Orbital_009	RIGHT	568,11 – 625,26	704,91 – 849,48
Orbital_010	RIGHT	759,24 – 1002,50	648,48 – 758,19
Orbital_011	LEFT	429,59 – 460,87	422,03 – 667,03
Orbital_012	LEFT	709,21 – 880,45	654,00 – 820,09

Source: the author, 2021.

5.1.2 Analysis of orbital floor defect – depth, length, and surface area

Here the measurements followed the same protocol that was used for total orbital floor. The measurement and the results of depth and length for the orbital floor defects using sagittal and coronal view respectively are presented on figure and table below. The method used for these measurements was the same as presented on figure 21.

Figure 24: Measurement of depth and length of orbital floor defect using sagittal and coronal views by VGSTUDIO MAX – Patient Orbital – 002. Red arrow shows depth measurements and blue arrow shows length measurements, and in which direction they appear on each screen of the software. The green lines are the ones measured on the software. Solid arrows are the ones placed on the exact CT slice of the images; dot arrows are the ones place in different CT slices.

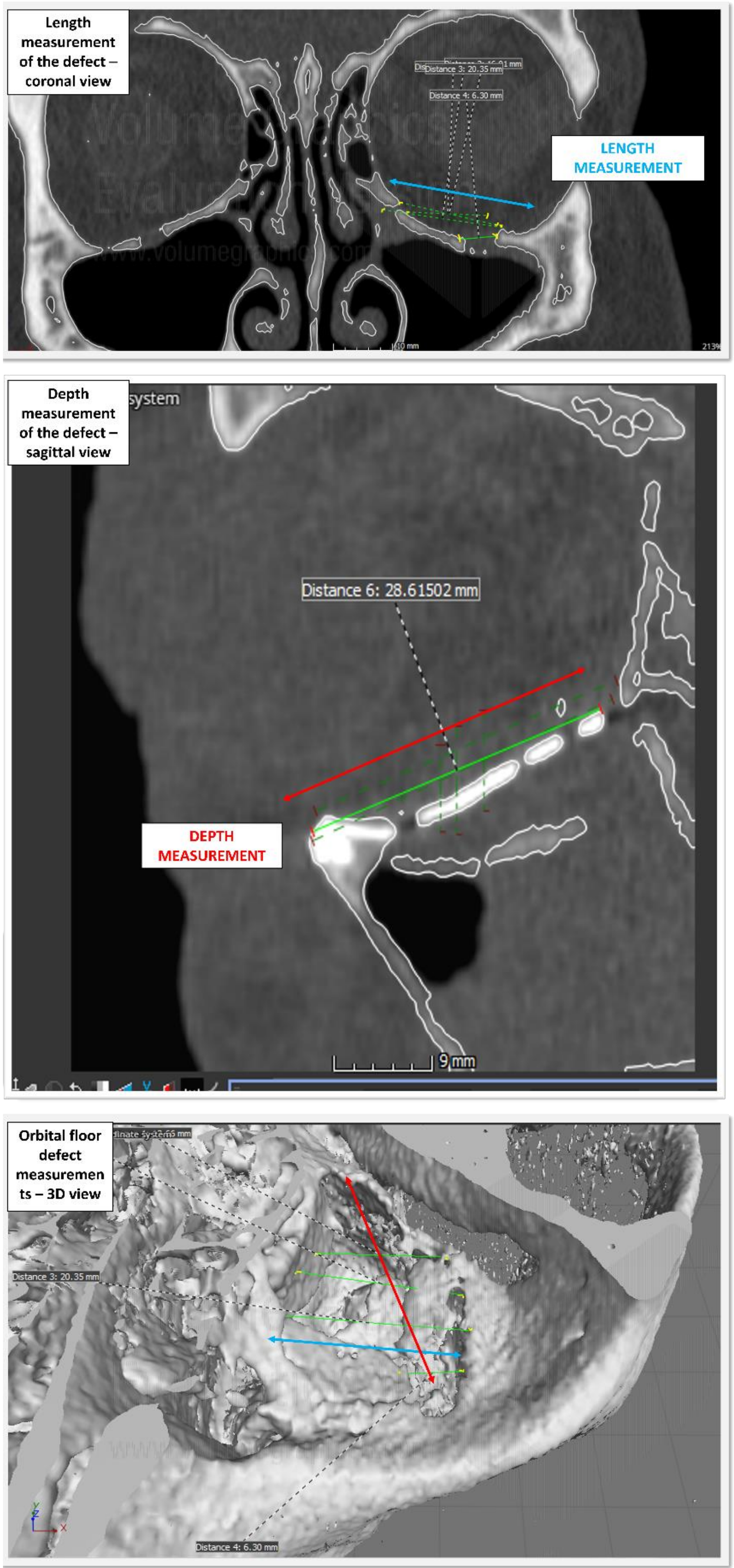

Source: the author, 2021.

Since the defects are not a round shape like the orbital floor itself and they may have varied sizes in different parts, for measuring their depth and their length, it was necessary to roll for different slices of the CT / DVT scans. And because of that, their values were not so similar comparing one to another like it was for the results of total orbital floor measurements.

Table VI: Results of measurements range of depth and length of orbital floor defects using sagittal and coronal view.

PATIENT ID	DEFECT SIDE	ORBITAL FLOOR DEFECTS	
		LENGTH [mm]	DEPTH [mm]
Orbital_001	BOTH	x	X
Orbital_002	LEFT	6,30 – 20,35	16,36 – 22,26
Orbital_003	RIGHT	x	X
Orbital_004	RIGHT	12,56 – 17,51	16,69 – 26,96
Orbital_005	LEFT	5,76 – 20,25	8,13 – 17,40
Orbital_006	LEFT	3,48 – 6,64	8,64 – 25,49
Orbital_007	RIGHT	6,04 – 16,06	4,46 – 19,35
Orbital_008	LEFT	10,00 – 21,64	12,12 – 24,96
Orbital_009	RIGHT	24,22 – 24,65	28,61 – 30,21
Orbital_010	RIGHT	9,43 – 17,71	9,57 – 21,75
Orbital_011	LEFT	6,42 – 13,97	6,53 – 19,43
Orbital_012	LEFT	14,19 – 20,10	14,35 – 27,86

Source: the author, 2021.

Orbital - 001 and Orbital - 003 could not be measured the defects depth and length because the images generated on VGSTUDIO MAX formed images with several holes all over the orbital floor, making it impossible to make a correct measurement since it was not possible to identify what were the broken bones parts. One possible explanation is that the thickness of the bones structure area for these patients could be very small, i.e., below the resolution limit, 400 µm.

The orbital floor lacks a rigid anatomic definition. It is generally agreed on that the floor consists of portions of the zygoma, maxilla, and palatine bones. The portions of these bones making up the floor are extremely thin and thus often difficult to completely visualize on CT imaging. Fractures of the floor often extend into the medial and lateral orbital walls. In addition, the position of the globe within the orbit makes visualization of the entire fracture extent difficult. Thus, a means of obtaining exact fracture dimension is lacking. However, it is widely agreed on that CT imaging represents the best noninvasive means of information regarding orbital floor anatomy (MANCHIO, 2010).

Figure 25: 3D image view generated by VGSTUDIO MAX, showing the presence of several holes and discontinuities.

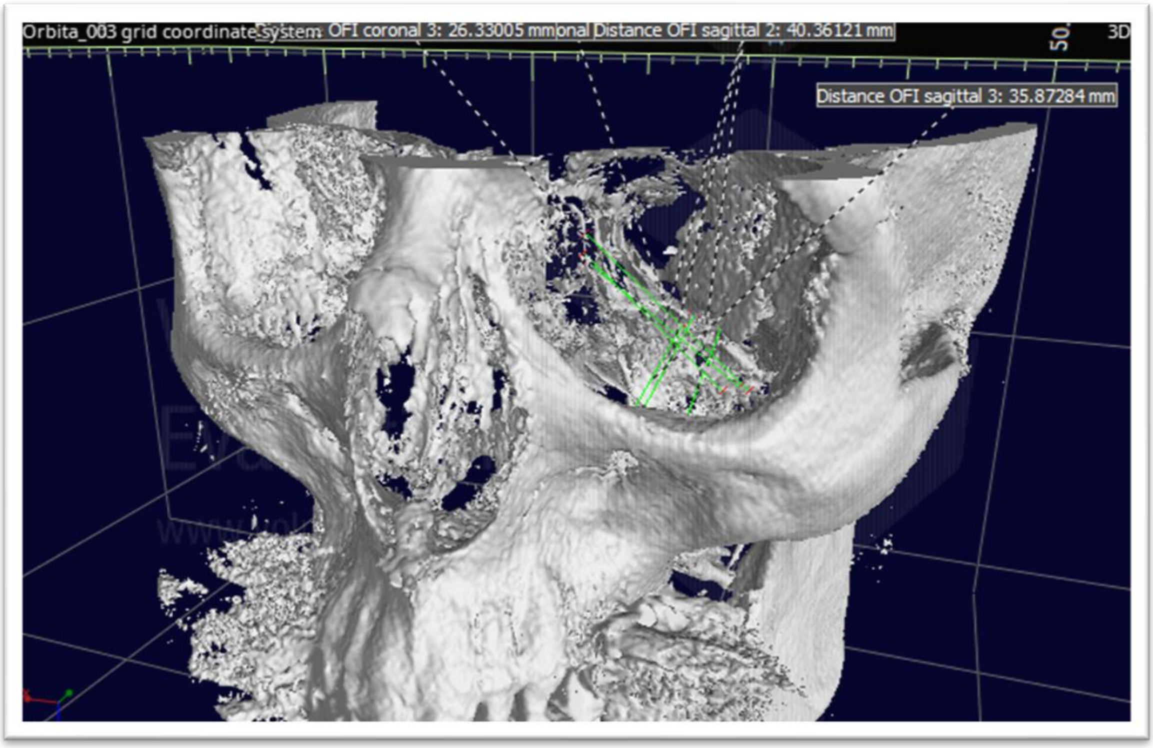

Source: the author, 2021.

A know systematic error is introduced by the CT scanner called “partial volume averaging”. This effect tends to modify density values at the osseous boundaries of anatomic structures and “blur” structures running obliquely through a scan section. Consequently, higher region of interest values in superior and inferior orbital sections occur due to accumulated errors near the osseous margin of the orbital roof and floor (MANSON et al, 1986).

The maximum width or depth may not be accurate if the slice thickness of the CT scan images is too wide. Furthermore, knowledge of the maximum fracture width and depth is not as useful clinically as knowledge of the surface area (ANG et al, 2015).

The measurement and the results of orbital floor defects surface area are presented on figure and table below. The table also presents the maximum length and depth using the surface area created.

Figure 26: Total orbital floor defect surface area drawing suing transverse view on VGSTUDIO MAX using polyline tool – Patient **Orbital – 010.**

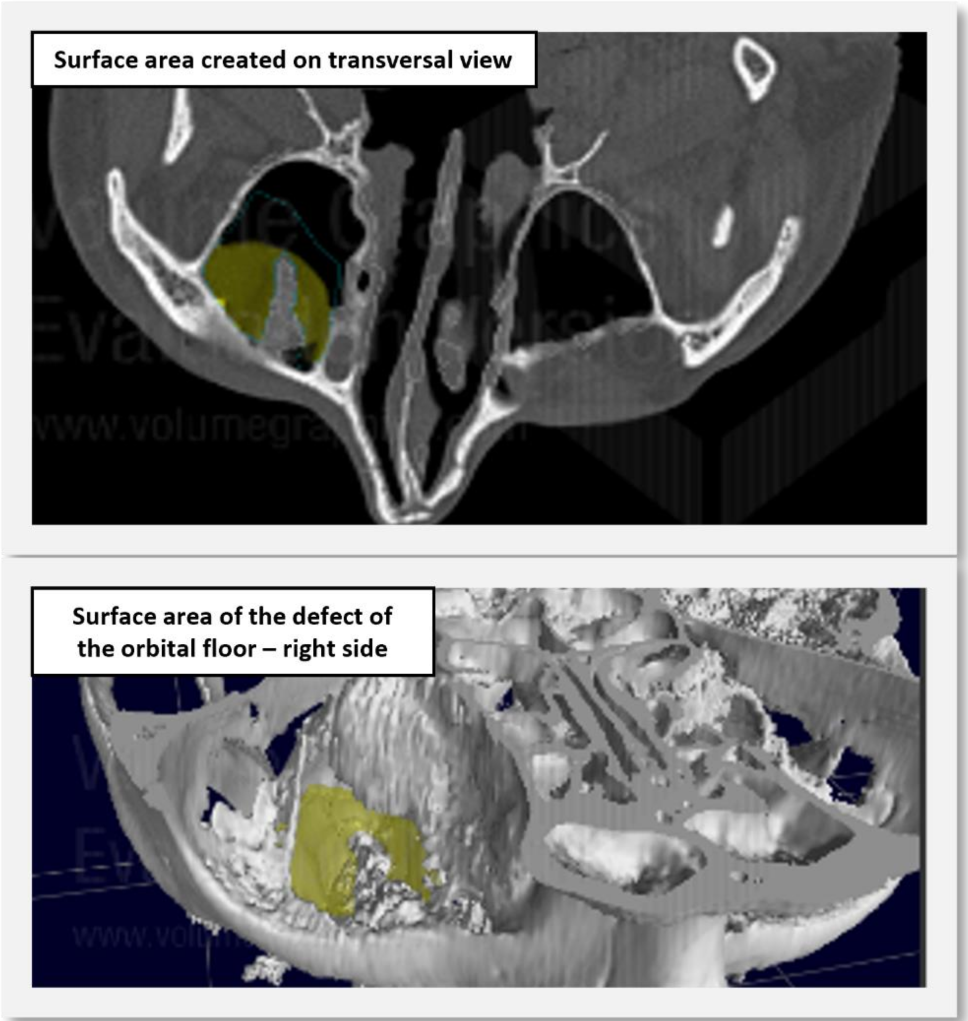

Source: the author, 2021.

Table VII: Results of measurements range of orbital floor defect (OFD) surface area and maximum depth and length using the surface area obtained.

PATIENT ID	DEFECT SIDE	OFD SURFACE AREA [mm²]	MAXIMUM LENGTH [mm]	MAXIMUM DEPTH [mm]
Orbital_001	BOTH	x	x	x
Orbital_002	LEFT	267,69 – 357,99	9,36 – 19,45	25,68 – 28,71
Orbital_003	RIGHT	x	x	x
Orbital_004	RIGHT	325,22 – 362,98	17,67 – 21,65	23,26 – 25,58
Orbital_005	LEFT	285,50 – 366,02	15,78 – 18,9	21,24 – 25,91
Orbital_006	LEFT	415,44 – 458,02	20,15 – 23,46	36,83 – 37,80
Orbital_007	RIGHT	203,36 – 220,24	15,16 – 19,76	16,74 – 27,12
Orbital_008	LEFT	566,34 – 595,56	22,00 – 25,65	28,92 – 36,79
Orbital_009	RIGHT	306,35 – 401,77	21,17 – 21,50	25,61 – 31,75
Orbital_010	RIGHT	485,83 – 584,68	22,19 – 25,48	34,55 – 37,67
Orbital_011	LEFT	260,15 – 359,85	21,10 – 26,19	15,50 – 27,65
Orbital_012	LEFT	517,7 – 626,14	23,61 – 25,49	27,41 – 28,82

Source: the author, 2021.

Here, the same problem mentioned before applies again for Orbital – 001 and Orbital – 003, since they could not be measured.

5.2 STATISTIC EVALUATION

The statistical analysis is divided in two parts: first for total orbital floor measurements and second for orbital floor defects measurements, the las part being compared with other literature results.

5.2.1 Total orbital floor evaluation

The graphics below show the comparison of measurements of length and depth between left and right side of each of twelve anonymized patient's CT/DVT scans that were used for this work.

Figure 27: Comparison between length measurements of left side of total orbital floor for all patients in [mm].

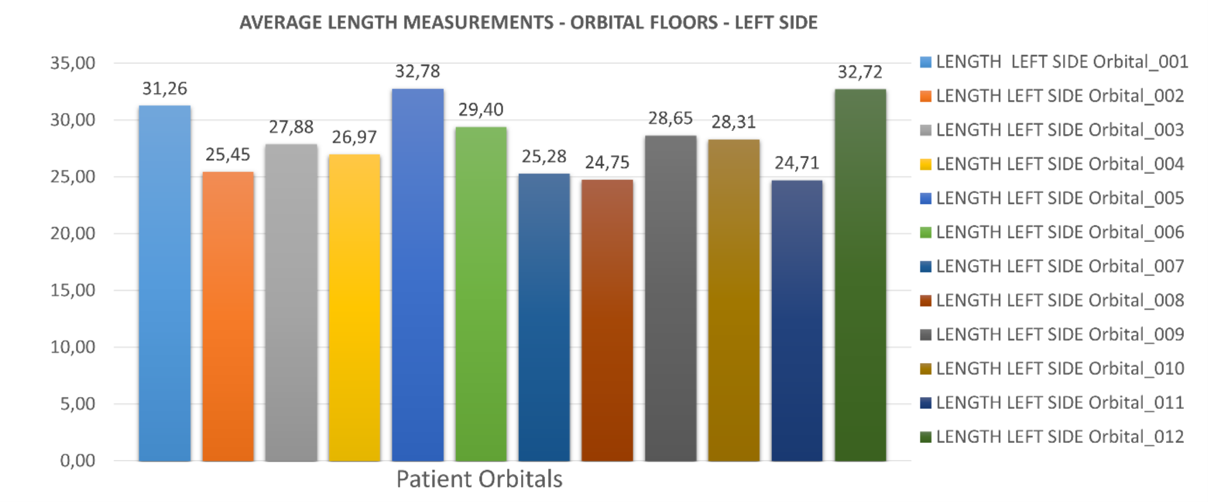

Source: the author, 2021.

Figure 28: Comparison between length measurements of right side of total orbital floor for all patients in [mm].

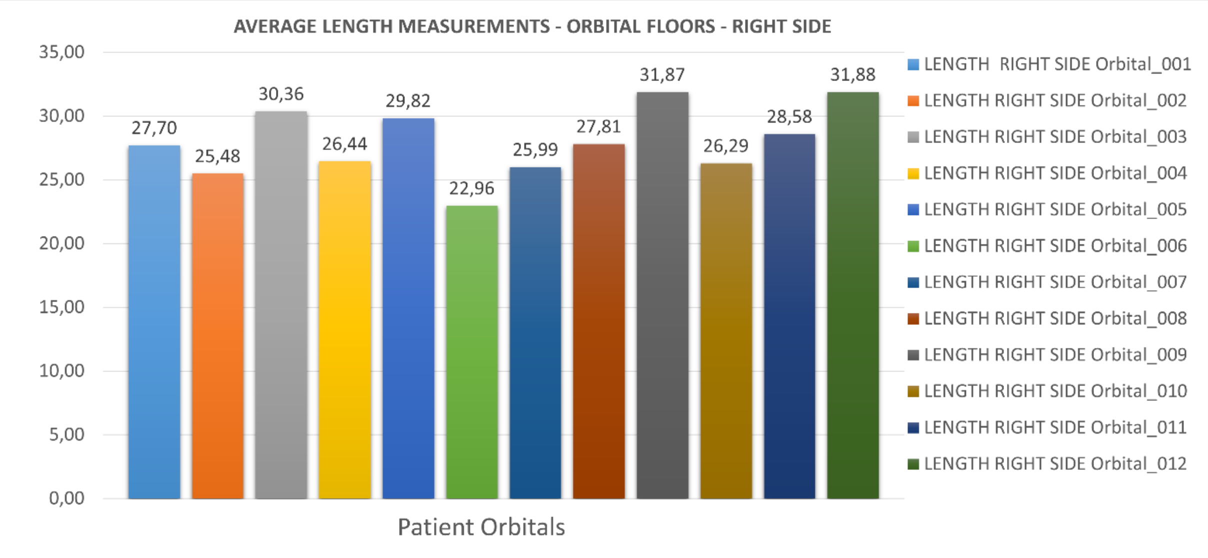

Source: the author, 2021.

It is possible to see that for the length measurements the values stick on the interval of 24,71 to 32,78 mm considering the left side of orbital floors and for the right side the interval is from 22,96 to 31,88 mm (p = 0,83).

Figure 29: Comparison between depth measurements of left side of total orbital floor for all patients in [mm].

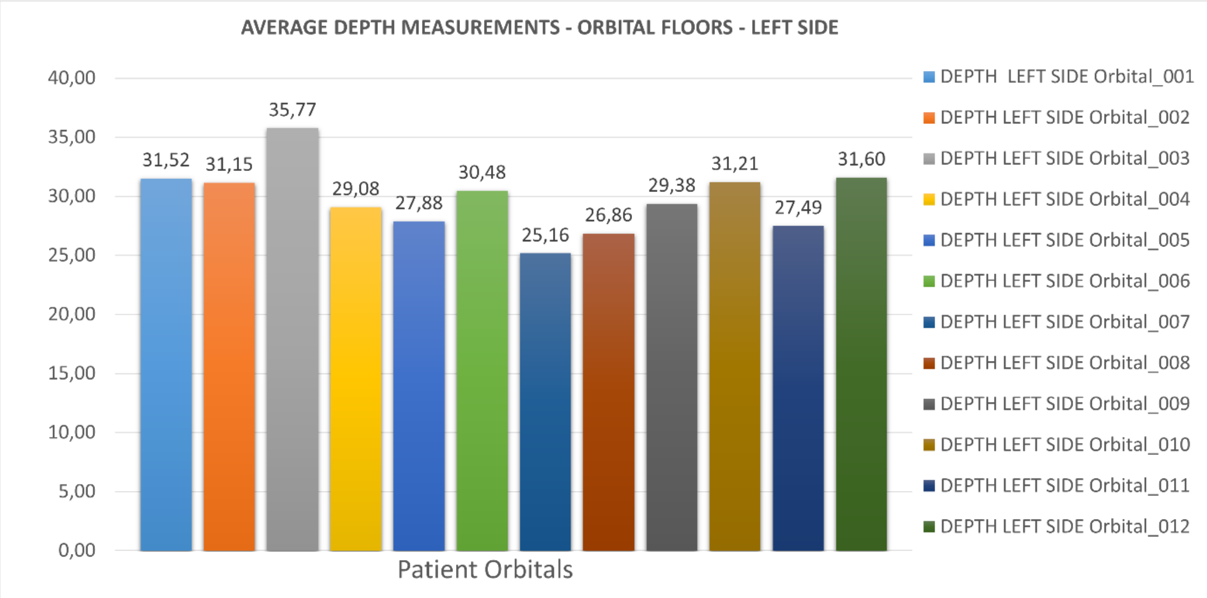

Source: the author, 2021.

Figure 30: Comparison between depth measurements of right side of total orbital floor for all patients in [mm].

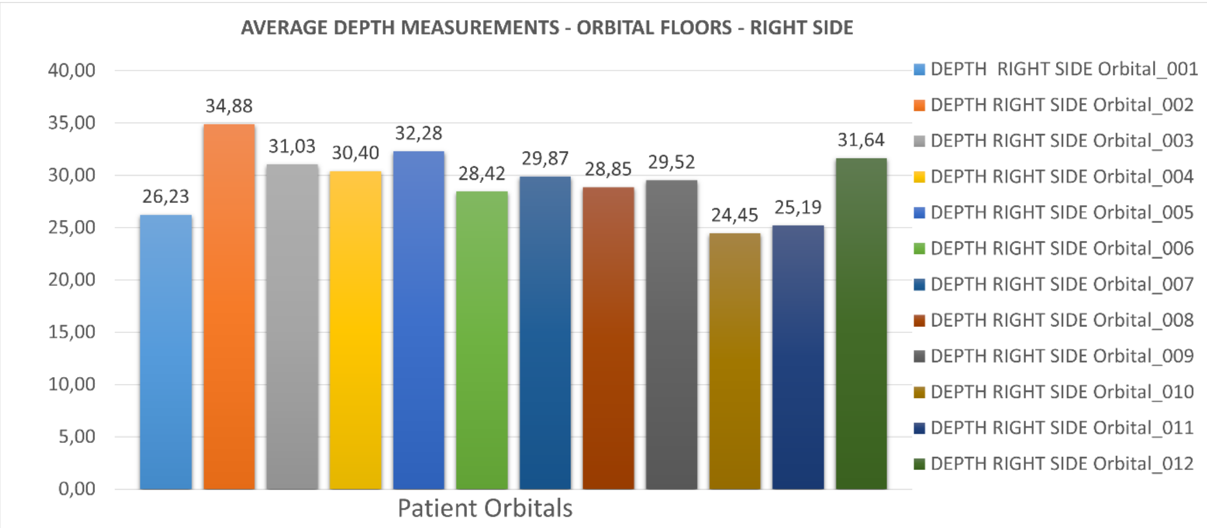

Source: the author, 2021.

For the depth measurements the values stick on the interval of 25,16 to 35,77 mm considering the left side of orbital floors and for the right side the interval is from 24,45 to 34,88 mm (p = 0,74). The statistical analysis made for each of the four types of measures is as follows.

Table VIII: Mean value and Student's t - test obtained for length and depth measurements of left and right sides of total orbital floor area.

MEAN VALUE (mm)

	LEFT SIDE (n=12)	RIGHT SIDE (n=12)	*p* – value (Student's t - test)
LENGTH	28,18 ± 2,93	27,93 ± 2,70	0,83
DEPTH	29,80 ± 2,80	29,40 ± 3,03	0,74

Source: the author, 2021.

The mean value for all measurements is very similar and the *p*-value confirms it, being bigger than 0,05. No studies were found to compare these measurements results.

The total surface area measurements for left and right side of orbital floors are presented as follow:

Figure 31: Comparison between total surface area measurements of left side of orbital floor for all patients in [mm²].

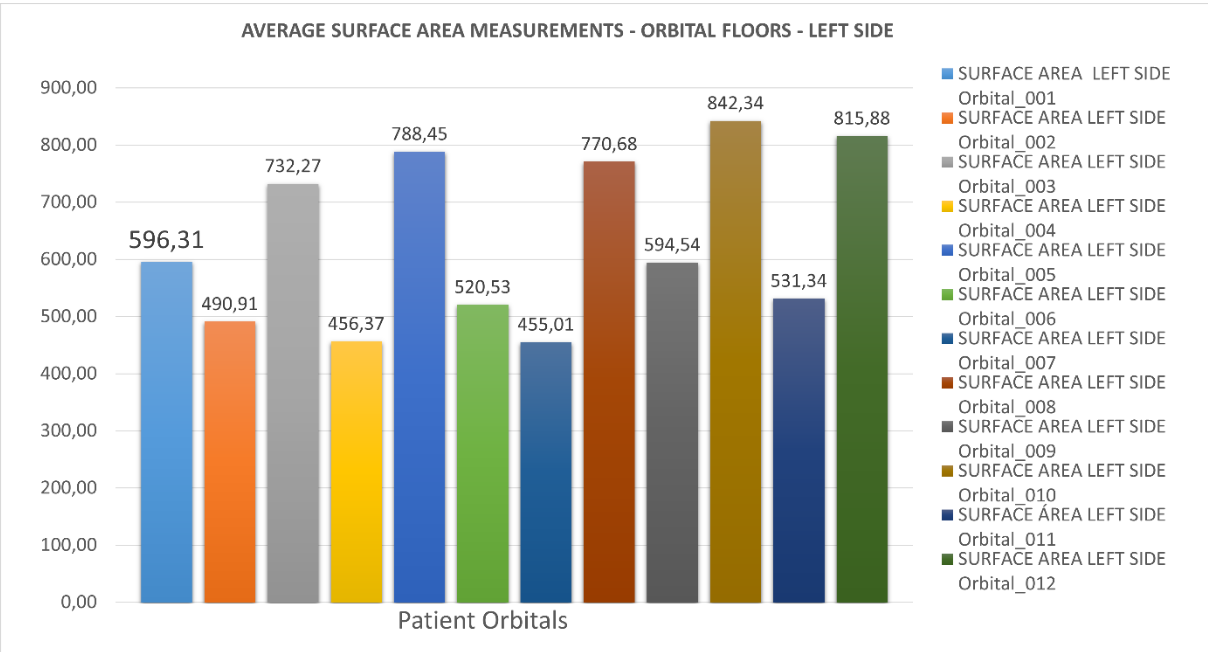

Source: the author, 2021.

The total surface area measurements values stick on the interval of 455,01 to 842,34 mm² considering the left side of orbital floors and for the right side they stay between 427,90 and 873,12 mm (*p* = 0,88). They vary more than length and depth because depending on the slice selected to create the points the variation in mm² will be greater than in mm, but even so they stay within a small range of values of the same order of magnitude.

Figure 32: Comparison between total surface area measurements of left right of orbital floor for all patients in [mm²].

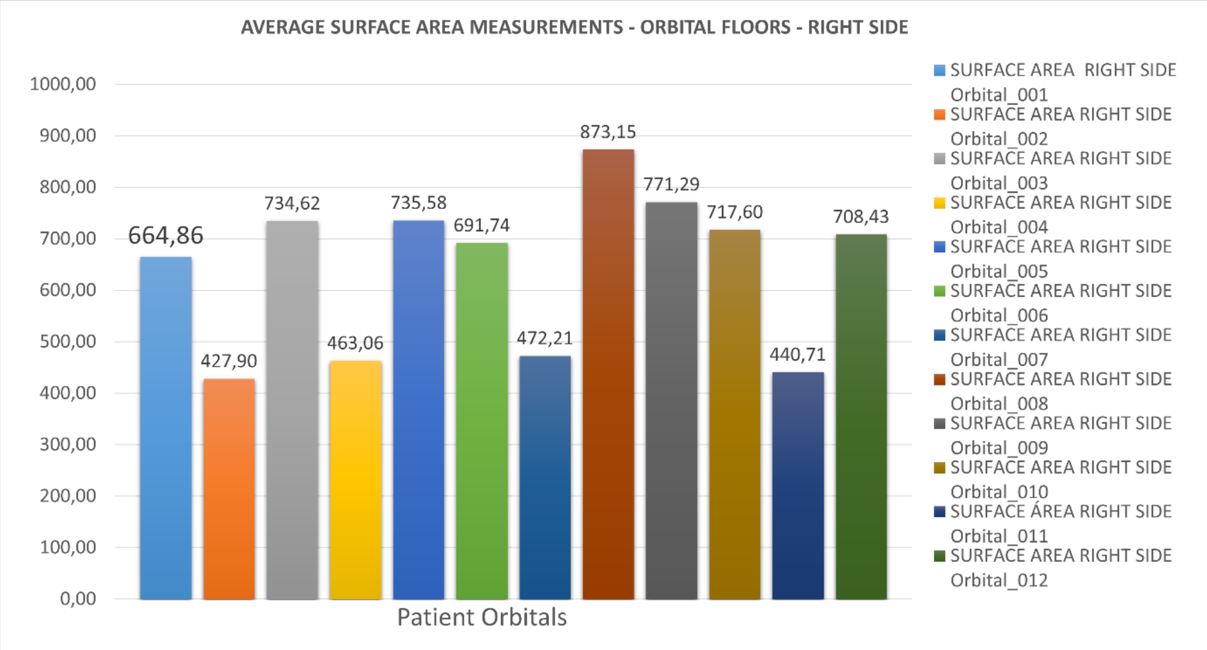

Source: the author, 2021.

The statistical analysis made for orbital floor total surface areas is as follows:

Table IX: Mean value and Student's t - test obtained for total surface area measurements of left and right side.

MEAN VALUE (mm²)

	LEFT SIDE (n=12)	RIGHT SIDE (n=12)	*p* – value (Student's t - test)
SURFACE AREA	632,89 ± 147,44	641,76 ± 150,09	0,88

Source: the author, 2021.

The mean value for left and right side are very similar, and the *p*-value confirms that are no differences between them with statistical significance. Some studies were found in literature that also measure the total orbital floor area (PLODER et al, 2002, 2003; SCHOUMAN et al, 2012; ROUL-YVONNET, 2017). A comparison table is also presented below showing number of patients, total surface area, range of values and type of measurement – using transversal, sagittal or coronal view.

Table X: Mean value ± SD comparisons with other literature for surface area measurements of total orbital floor surface (OBF).

AUTHOR AND YEAR	NUMBER OF PATIENTS (n)	Mean value ± SD SURFACE AREA OBF [mm²]	RANGE [mm²]	TYPE OF MEASUREMENT
Author of this work, 2021	10	637,32 ± 145,57	427,90 – 873,15	Transversal view
PLODER et al, 2002	38	572,00 ± 107,00	343,00 – 769,00	Coronal view
PLODER et al, 2003	30	604,00 ± 98,00	417,00 – 746,00	Coronal view
SCHOUMAN et al, 2012	10	645,00 ± 67,00	450,00 – 800,00	Coronal view
ROUL-YVONNET et al, 2017	90	588,00 ± 87,00	319,00 – 782,00	Coronal view

Source: the author, 2021.

All results are in similar ranges of values and the most similar study with the present work considering means value + SD and range is from SCHOUMAN et al, 2012, being the type of measurement the only difference.

5.2.2 Orbital floor defects evaluation

The graphics below show the comparison of measurements of length and depth of the orbital floor defects of ten from the twelve anonymized patient’s CT/DVT scans that were used for this work.

Figure 33: Comparison between measurements of length and depth of orbital floor defects for all patients in [mm].

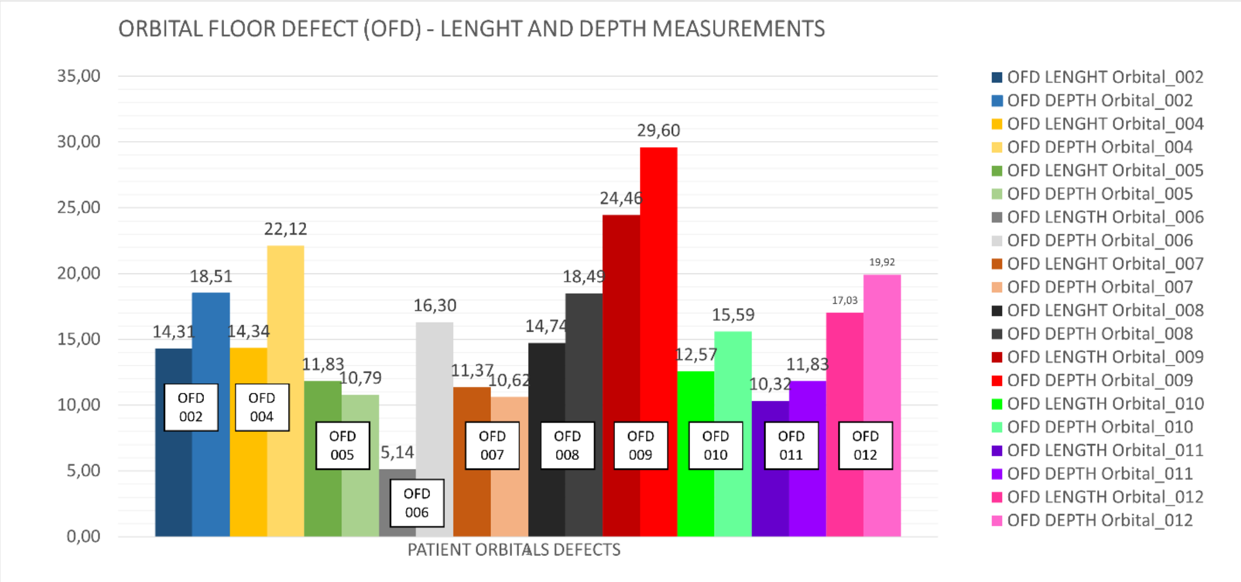

Source: the author, 2021.

The statistical analysis obtained for each of measurement of orbital floor defects is as follows:

Table XI: Mean value and Student's t - test for length and depth measurements of orbital floor defects (OFD).

MEAN VALUE (mm)

	LENGTH (n=10)	DEPTH (n=10)	*p* – value (Student's t - test)
OFD	13,61 ± 4,98	17,38 ± 5,82	0,14

Source: the author, 2021.

As it is shown above, these values have a much bigger range, since each fracture size is unique and dependent of the patient and causes for the damage going from 5,14 mm to 24,50 mm for length measurements and from 11, 83 mm to 29,60 mm for depth measurements. This can be notice with the high standard deviation values. The *p*-value shows that the mean differences are not statistically significant. Furthermore, here it is worth noting that as mentioned earlier, it was not possible to analyze the fractures of patients 001 and 003, so they are not shown in the graph. No studies were found to compare the results.

The comparison of orbital floor defects surface area measurements for all patients is presented below:

Figure 34: Comparison between orbital floor defect measurements of surface area for all patients in [mm²].

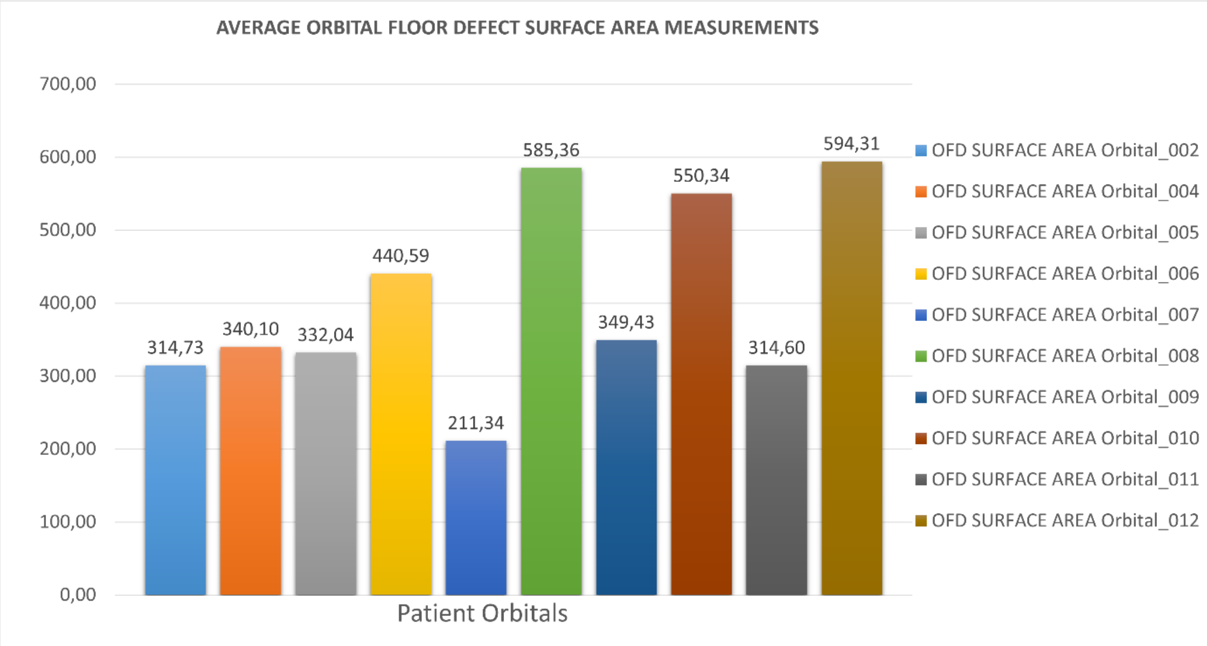

Source: the author, 2021.

Different methods for the assessment of orbital floor defect surface area considering it as a plane surface and using CT scans techniques can be found in literature. The mean value obtained in this work for orbital floor defect area is very similar with other studies that used computational protocols as well (ANG et, 2015; CORNELIUS et al, 2020; PLODER et al, 2002, 2003; SCHOUMAN et al, 2012; ROUL-YVONNET et al, 2017). A comparison graphic for the average of orbital floor defect surface areas is presented below. A comparison table is also presented below showing number of patients, defect surface area, range of values and type of measurement – using transversal, sagittal or coronal view.

Figure 35: Comparison with literature of orbital floor defect surface area in [mm²].

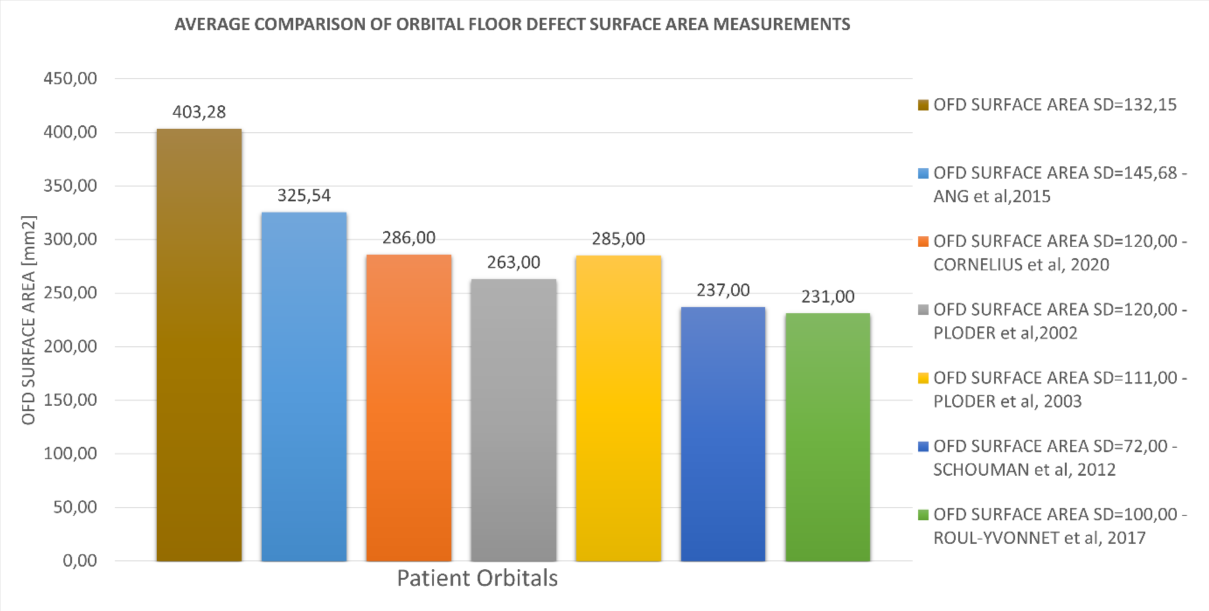

Source: the author, 2021.

Table **XII: Mean value ± SD comparisons with other literature for surface area measurements of orbital floor defects (OFD).**

AUTHOR AND YEAR	NUMBER OF PATIENTS (n)	Mean value ± SD SURFACE AREA OFD [mm²]	RANGE [mm²]	TYPE OF MEASUREMENT
Author of this work, 2021	10	403,28 ± 132,15	211,34 - 594,31	Transversal view
ANG et al, 2015	03	325,54 ± 145,69	121,80 - 461,90	Coronal view
CORNELIUS et al, 2020	137	286,00 ± 120,00	110,00 – 609,00	Coronal view
PLODER et al, 2002	38	263,00 ± 120,00	40,00 – 577,00	Coronal view
PLODER et al, 2003	30	285,00 ± 111,00	40,00 – 485,00	Coronal view
SCHOUMAN et al, 2012	10	237,00 ± 72,00	64,00 – 401,00	Coronal view
ROUL-YVONNET et al, 2017	90	231,00 ± 100,00	13,00 – 453,00	Coronal view

Source: the author, 2021.

The study that matches most closely with the present work is the one made by ANG et al, 2015. Even though the range values are similar, this study had a higher mean value of them all. This can be explained with the small number of patients involved on the measurements along with the size of the defects that were bigger - and there is no prediction in that. The main difference from this work with all others compared is the measurement type that here were made using transversal view instead of using coronal slices and could be an explanation why the results are bigger, since the accuracy of the area limits are not so good as in the coronal view.

Finally, a ratio comparison (in percentage) between total surface area and defect surface area is presented below:

Table XIII: Ratio between total orbital floor surface (OFS) area and orbital floor defect (OFD) surface area.

PATIENT	OFS / OFD [%]
Orbital_002	63,00
Orbital_004	73,00
Orbital_005	45,00
Orbital_006	85,00
Orbital_007	45,00
Orbital_008	76,00
Orbital_009	46,00
Orbital_010	77,00
Orbital_011	63,00
Orbital_012	74,00

Source: the author, 2021.

This analysis shows that the orbital floor fractures represent at least 45% of the total area of the orbital, highlighting the importance of the study on this subject. It confirms the need to perform fracture measurements for each specific patient for the treatment to be more effective at each case and with less chance of problems or complications. The studies mentioned before also reported ratio results between total orbital floor area and orbital floor defect area (PLODER et al, 2002, 2003; SCHOUMAN et al, 2012; ROUL-YVONNET, 2017). The table below shows the comparison:

Table XIV: Mean value + SD for ratio between total orbital floor surface (OFS) area and orbital floor defect (OFD) surface area.

AUTHOR AND YEAR	NUMBER OF PATIENTS (n)	Mean value ± SD OFS / OFD [%]	TYPE OF MEASUREMENT
Author of this work, 2021	10	65,00 ± 15,00	Transversal view
PLODER et al, 2002	38	45,30 ± 17,60	Coronal view
PLODER et al, 2003	30	46,60 ± 15,70	Coronal view
SCHOUMAN et al, 2012	10	36,60 ± 10,70	Coronal view
ROUL-YVONNET et al, 2017	90	39,00 ± 14,00	Coronal view

Source: the author, 2021.

The mean value for defect and total area ratio obtained on this work is higher than the ones calculated on the other studies, which can be expected since the defect surface areas values measured here were also higher.

5.2.3 Errors to be considered in the assessment or orbital floor and its defects

Two mainly source errors can affect the analysis: the one's from the evaluator and the one's from the software used. The evaluator in this work had never before analyzed any type of CT / CBCT scans of orbital floor fractures, needing to study from the basic concepts. However, the protocol used as guide for these measurements was one that used observers without clinical experience in orbital fracture detection (ANG et al, 2015), and as showed above, the results obtained here agreed with the ones obtained on their study. The biggest difference is that they had several different evaluators and here just one evaluator was used, which can increase de possible errors since the sample is much smaller, and one mistake could be made for all the measurements.

For all measurements made, it was considered that the orbital floor is a plane surface, which its known that it does not apply, being a 3D surface with contours, therefore this induces some value errors in the ones obtained.

The possible errors from the software relied on parameters that were set, such as resolution and grey values used for determining which is bone tissue and which is soft tissue. Some of the parameters were set as indicated in the tutorial documents provided by the software creator and therefore, they may not be the best option for this type of measurement. Another source of error inside the software limitations it that the surface areas were calculated using transversal view, differently from most of literature studies that uses coronal and sagittal view directly. It is notable that the surface area values obtained in this work were a little higher than the results compared with literature, and this can may be explained with this. A top view for surface area could involve more mm^2 than it actually has the area of interest.

Although there are still some limitations in measuring orbital area, it is a common sense in literature that CT scans are the most reliable technique to analyze preoperatively fractures with minimal invasion on the patient. The need of pre-operative analysis of orbital floor blowout fractures and the use of available software's is extremely important, since once the size and shape of the defect is mapped, the patient can have a specific shapeable implant which will improve his/her life quality.

6 CONCLUSIONS

The analysis of orbital floor blowout fractures using anonymized computed tomography (CT) and cone beam computed tomography (CBCT) scans was done. The study of orbital floor and orbital floor blowout fractures were made to understand the etiology, treatment, and possible material implants for this type of defects. The analysis of orbital defects was done, and the defects were measured considering their depth, length and surface area using the software VGSTUDIO MAX by Volume Graphics. The method was successfully done using VGSTUDIO MAX for the measurements, it is possible to learn relatively quick how to use the software and how to do the measurements of orbital floor and orbital floor defects, even if the person is new in this subject. However, it is important to note that this study is preliminary for the software for this use, in which a small sample of patients was used for the analysis and just one person tested the method.

The main values obtained for length measurements of total orbital floor were 28,18 ± 2,93 mm and 27,93 ± 2,70 mm for left and right side respectively (p = 0,83). The main values obtained for depth measurements of total orbital floor were 29,80 ± 2,80 mm and 29,40 ± 3,03 mm for left and right side respectively (p = 0,74). The main values obtained for length and depth of orbital floor defects were 13,61 ± 4,98 and 17,38 ± 5,82 respectively (p = 0,14). By conventional criteria, these differences are considered to be not statistically significant showing reproducible results, however, no studies were found to compare it with. The results obtained on this work for surface defect area are similar to values obtained in literature, being closest to the ones obtained on the protocol proposed by ANG et Al (2015). The values of surface area defects stayed between 211,34 and 594,31 mm^2 and ANG et al (2015) obtained values between 121,80 and 461,90 mm^2. The main values obtained for total surface area were 632,89 ± 147,44 mm^2 and 641,76 ± 150,09 mm^2 for left and right side respectively (p = 0,88). All results are in similar ranges of values for orbital floor total surface area and the most similar study with the present work considering means value + SD and range is from SCHOUMAN et al, 2012, being the type of measurement the biggest difference between them. The main value obtained here was 637,32 ± 145,57 and the main value in SCHOUMAN et al, 2012 was 645,00 ± 67,00. The mean value for defect and total area ratio obtained on this work, 65,00 ± 15,00, a little higher than the ones calculated on the other studies found in literature, which can be expected since the defect surface areas values measured here were also a little higher.

It was not possible to perform defect measurements in two patients with CBCT/DVT datasets because the images generated by the software were not with good resolution, possibly because the bone structures on these cases are smaller than the thickness limit resolution. Finally, the present study encourages the use and study of available software's for CT image analysis for orbital floor and orbital floor fractures, this being of great help in deciding the treatment to be followed and in choosing the best specific implant patient.

7 FUTURE WORKS

- To validate the software for the intended use presented on this work, it is recommended to have a bigger number of patients with orbital floor fractures and analyze their CT scans, print their orbital floor areas, measure the real defect, and compare with software results;
- Do measurements using the 3D view and considering the original shape of the orbital floor for the surface area;
- Try the method with different users to analyze the difficult to make the measurements in the software;
- Calculate the volume of orbitals to compare defect and non-defect ones;
- Study of the resolution and parameters that could be improved to have a better 3D reconstruction using the software and consequently an even more accurate measurement result;
- Use .stl data to print 3D models of orbital area and orbital floor defect from the reconstruction model obtained on VGSTUDIO MAX.

8 REFERENCES

ANG, C. H. A.; LOW, J. R.; SHEN, J. Y.; CAI, E. Z. Y.; HING, E. C. H.; CHAN, Y. H.; SUNDAR, G.; LIM, T. C. **A Protocol to Reduce Interobserver Variability in the Computed Tomography Measurement of Orbital Floor Fractures**. Craniomaxillofacial Trauma Reconstruction. 8:289–298. 2015.

ABRAMOVITCH, K.; DWIGHT, D. R.; **Basic Principles of Cone Beam Computed Tomography**. Dental Clinics of North America Volume 58, Issue 3, Pages 463-484 2014.

BAINO, F. **Biomaterials and implants for orbital floor repair**. Acta Biomaterialla, Elsevier Journal. 7 3248 – 3266. 2011.

BERTOL, L. S. **Contribuição ao Estudo da Prototipagem Rápida, Digitalização Tridimensional e Seleção de Materiais no Design de Implantes Personalizados**. Dissertação de Mestrado – Porto Alegre: Universidade Federal do Rio Grande do Sul, Escola de Engenharia, Programa de Pós-Graduação em Engenharia de Minas, Metalúrgica e de Materiais, 2008.

BOYD, K. **What Is an Orbital Fracture?** American Academy of Ophthalmology. 2017 <https://www.aao.org/eye-health/diseases/what-is-orbital-fracture> Accessed in october 2021.

BOYETTE, J. R.; PEMBERTON, J. D.; BONILLA-VELEZ, J. **Management of orbital fractures: challenges and solutions**. Clinical ophthalmology (Auckland, N.Z.), 9, 2127–2137, 2015.

CORNELIUS, C.P.; STIEBLER, T.; MAYER, P.; SMOLKA, W.; KUNZ, C.; HAMMER, B.; JAQUIÉRY, C.; BUITRAGO-TÉLLES, C.; LEIGGENER, C.S.; METZGER, M.C.; WILDE, F.; AUDIGÉ, L.; PROBST, M.; STRONG, E.B.; CASTELLETTI, N.; PREIN, J. PROBST, F.A. **Prediction of surface area size in orbital floor and medial orbital wall fractures based on topographical subregions**. Journal of Cranio-Maxillofacial Surgery, Volume 49, Issue 7, Pages 598-612, 2021.

DUBOIS, L. **Predictability in orbital reconstruction**. (PhD thesis) Faculty of Dentistry (ACTA), University of Amsterdam, 2016.

EGGERS, G.; KLEIN, J.; WELZEL, T.; MÜHLING, J. **Geometric accuracy of digital volume tomography and conventional computed tomography.** British Journal of Oral and Maxillofacial Surgery. 46 (2008) 639–644, 2008.

GANDER, T.; ESSIG, H.; METZLER, P.; LINDHORST, D.; DUBOIS, L.; RÜCKER, M.; SCHUMANN, P. **Patient specific implants (PSI) in reconstruction of orbital floor and wall fractures**. Journal of Cranio-Maxillofacial Surgery, 2014.

GUNARAJAH, D. R.; SAMMAN, N. **Biomaterials for repair of orbital floor blowout fractures: a systematic review**. American Association of Oral and Maxillofacial Surgeons. Journal of Oral Maxillofacial Surgery 71:550-570. 2013.

HOYT , C. S.; TAYLOR, D. **Pediatric Ophthalmology and Strabismus.** (Fourth Edition), Pages 690-699. 2013.

JAQUIÉRY, C; AEPPLI, C.; CORNELIUS, P.; PALMOWSKY, C; KUNZ, B.; HAMMER, B. **Reconstruction of orbital wall defects: critical review of 72 patients**. Journal of Oral & Maxillofacial Surgery, Nr. 36, pp. 193-9. 2007.

JIANG, T.; **Development and construction of test rigs for mechanical testing of fiber reinforced material composites for reconstruction of the bony orbita**. Internship thesis. Leibniz-Institut für Polymerforschung Dresden e. V. 2020.

KHAN A. M, VARVARES, MA. **Traditional approaches to the orbit**. Otolaryngol Clin North Am. 39(5):895-909. 2006.

KIM, YH; PARK, Y.; CHUNG, K.J. **Considerations for the Management of Medial Orbital Wall Blowout Fracture**. Archives of plastic surgery vol. 43,3: 229-36. 2016.

MANCHIO, J. V., SATI, S., ROSMAN, D. A., BRYAN, D. J., Lee, G. M., & WEINZWEIG, J. **Role of Sagittal Reformatted Computed Tomographic Images in the Evaluation of Orbital Floor Fractures**. Journal of Craniofacial Surgery, 21(4), 1153–1157. 2010.

MANSON, P. N. M.D.; GRIVAS, A. M.A.; ROSENBAUM, A. M.D.; VANNIER, M. M.D.; ZINREICH, J.M.D.; ILIFF, N. M.D. **Studies on Enophthalmos: II. The Measurement of Orbital Injuries and Their Treatment by Quantitative Computed Tomography**. Plastic and Reconstructive Surgery: Vol. 77 - Issue 2 - p 203-214. 1986.

Orbital rim. (n.d.) **Medical Dictionary**. 2009. from <https://medical-dictionary.thefreedictionary.com/orbital+rim> Accessed in October 202.

PLODER, O.; KLUG, C.; VORACEK, M.; BURGGASSER, G.; CZERNY, C.; **Evaluation of computer-based area and volume measurement from coronal computer tomography scans in isolated blowout fractures of the orbital floor**. Journal of Oral Maxillofacial Surgery. 30-1267-1272. 2002.

PLODER, O.; OECKHER, M.; KLUG, C.; VORACEK, M.; WAGNER, A.; BURGGASSER, G.; BAUMANN, A.; CZERNY, C.; **Follow-up study of treatment of orbital floor fractures: relation of clinical data and software-based CT-analysis**. Int J Oral Maxillofac Surg. 32-257-262. 2003.

RADIOPAEDIA <https://radiopaedia.org/articles/bony-orbit?lang=us> Accessed in October 2021.

RADIOPAEDIA <https://radiopaedia.org/articles/orbital-apex > Accessed in October 2021.

RHEE, J., KILDE, J., YOGANADAM, N. PINTAR, F. **Orbital floor blowout fractures**. American Medical Association. Journal of Facial Plastic Surgery. Volume 4, 2002.

ROUL-YVONNET, F.; GOLMARD, J.L.; GOUDOT, P.; SCHOUMAN, T. **Evaluation of a radiological score in the management of pure fractures of the orbital floor**. Journal of Craniofacial Surgery. 28: e344-e349. 2017.

ROTH, F. S.; KOSHY, J. C.; GOLDBERG, J. S.; & SOPARKAR, C. N. **Pearls of orbital trauma management.** Seminars in plastic surgery. 2010. 24(4), 398–410.

SCHOUMAN, T.; COURVOISIER, D.S.; IMHOLZ, B.; VAM ISSUM, C.; SCOLOZZI, P.; **Computational area measurement of orbital floor fractures: reliability, accuracy and rapidity.** Europe Journal of Radiology. 81: 2251-2254. 2012.

SHUNMWAY, C.L; MOTLAGH, M.; WADE, M. **Anatomy, Head and Neck, Orbit Bones**. StatPearls Publishing LLC. 2021. NBK531490 – 30285385. <https://www.ncbi.nlm.nih.gov/books/NBK531490/> Accessed in October 2021.

STRATOVAN. <https://www.stratovan.com/products/pro-surgical-3d> Accessed in April 2021.

VEHMEIJER, M.; EIJNATTEN, M.; LIBERTON, N., WOLFF, J**.; A novel Method of Orbital Floor Reconstruction Using Virtual Planning, 3-Dimensional Printing, and Autologous Bone**. Journal of Oral and Maxillofacial Surgery. 2016.

VIOZZI, C.F.; **Maxillofacial and Mandibular Fractures in Sports**. Clin Sports Med. 2017 Apr ;36(2):355-368. doi: 10.1016/j.csm.2016.11.007. PMID: 28314422.

TURVEY, T. A.; GOLDEN B. A.; **Orbital anatomy for the surgeon**. Oral Maxillofac Surg Clin North Am. 24(4):525-36. 2012.

WI, J.M.; SUNG, K.H.; CHI, M. **'Orbital volume restoration rate after orbital fracture'; a CT-based orbital volume measurement for evaluation of orbital wall reconstructive effect.** Eye. London, England. Vol. 31, 713–719. 2017.

Volume Graphics. <http://www.volumegraphics.com> Accessed in April 2021.